Supplementary Information

Phosphole Oxide-Based Cyclometalated Platinum(II) β-Diketonate Complexes for Cooperative Self-Assembly and Solution-Processable Resistive Memories with Excellent Stability

Andy Shun-Hoi Cheung, Eugene Yau-Hin Hong and Vivian Wing-Wah Yam*

Institute of Molecular Functional Materials and Department of Chemistry,

The University of Hong Kong, Pokfulam Road, Hong Kong, PR China

E-mail: wwyam@hku.hk

Experimental

Physical Measurements and Instrumentation

^{1}H NMR spectra were recorded on a Bruker AVANCE 400 (400 MHz) NMR spectrometers with chemical shifts relative to tetramethylsilane (Me_4Si). $^{31}P\{^{1}H\}$ NMR spectra were recorded on a Bruker AVANCE 400 NMR spectrometer with chemical shifts reported relative to 85 % phosphoric acid. High-resolution electrospray ionization (ESI) mass spectra were recorded on a Bruker maXisII high-resolution ESI-QTOF mass spectrometer. All elemental analyses were performed on a Flash EA 1112 elemental analyser by the Institute of Chemistry at the Chinese Academy of Sciences in Beijing. The X-ray diffraction data for the corresponding crystal structure were collected on the Bruker D8 VENTURE Photon100 CMOS X-Ray Diffractometer by using graphite monochromatized Mo K_α radiation (λ = 0.71073 Å) or on the Bruker D8 VENTURE MetalJet Photon II CMOS X-Ray Diffractometer by using graphite monochromatized Ga K_α radiation (λ = 1.34318 Å). UV-Vis absorption spectra were obtained by using a Varian Cary 50 UV/Vis spectrophotometer. Steady state excitation and emission spectra at 298 K and 77 K were recorded on a Spex Fluorolog-3 Model FL3-211 fluorescence spectrofluorometer equipped with a R2658P photomultiplier tube (PMT) detector. For solution state emission study, complexes were degassed on a high-vacuum line in a degassing cell with 10-mL Pyrex round-bottom flask connected by a sidearm to a 1-cm quartz fluorescence cuvette which were sealed from the atmosphere by a Bibby Rotaflo HP6/6 quick-release Teflon stopper. The samples were degassed with no fewer than four successive freeze-pump-thaw cycles. Emission lifetime measurements were performed using a conventional laser system. The excitation source used was the 355-nm output (third harmonic, 8 ns) of a Spectra-Physics Quanta-Ray Q-switch GCR-150 pulsed Nd-YAG laser (10 Hz). Powder X-ray diffraction data were collected on

Bruker D8 ADVANCE Powder X-ray Diffractometer in Bragg-Brentano ($\theta/2\theta$) reflection mode with a graphite monochromatized Cu-K_α radiation (λ = 1.54178 Å) and nickel filter. Transmission electron microscopy (TEM) experiments were performed on a Philips CM100 transmission electron microscope, while scanning electron microscopy (SEM) experiments were performed on a Leo 1530 Field-Emission-Gun scanning electron microscope. The selected area electron diffraction (SAED) experiments were performed on a FEI Tecnai G2 20 S-TWIN transmission electron microscope with an accelerating voltage of 200 kV. All experiments were performed at the Electron Microscopy Unit of The University of Hong Kong. All carbon-coated copper grids were pre-treated with a PELCO easiGlow Glow Discharge Cleaning System. Samples were prepared by dropping a few drops of solution onto the grids and dried by slow evaporation of the solvents. Dynamic light scattering (DLS) experiments were conducted at 298 K using a Malvern (UK) Zetasizer ZS90 with internal HeNe laser (λ_0 = 632.8 nm).

Nucleation–Elongation Model Studies

The melting curves obtained from the temperature-dependent UV-vis absorption studies were fitted to the nucleation–elongation model developed by Meijer and coworkers.[1] In this model, the nucleation and elongation regimes are governed by equations 1 and 2 respectively,

$$\phi_n = K_a^{1/3}\ exp\ [(2/3\ K_a^{-1/3} - 1)\frac{h_e}{RT_e^2}(T - T_e)] \quad (\mathbf{1})$$

$$\phi_n = \phi_{SAT}\ (1 - exp\ [-\frac{h_e}{RT_e^2}(T - T_e)]) \quad (\mathbf{2})$$

where ϕ_n is the degree of aggregation, h_e is the molecular enthalpy release during elongation, T_e is the elongation temperature, K_a is the dimensionless equilibrium constant of the nucleation step at T_e, ϕ_{SAT} is the parameter introduced to equate ϕ_n / ϕ_{SAT} to unity and R is the gas constant. The degree of aggregation of the complexes was deduced from the changes in the temperature-dependent UV-vis absorption studies (**8**, 500 nm; **10**, 550 nm) and by defining the degree of aggregation ϕ_n at the highest (333 K) and lowest (288 K) measured temperature as 0 and 1 respectively. $<N_n(T_e)>$, the number-averaged degree of polymerization averaged over all nucleated species at the elongation temperature is given by equation 3.[1]

$$<N_n(T_e)> = \frac{1}{k_a^{\frac{1}{3}}} \quad (\mathbf{3})$$

Fabrication and Characterisation of Resistive Memory Devices

Resistive memory devices were fabricated on an ITO-coated borosilicate glass substrate (2 cm × 2 cm) with a sheet resistance of 30 Ω square^{-1}. The substrates were first cleaned with Decon 90, rinsed with deionized water, followed by ultrasonication successively with deionised water, acetone, isopropanol and absolute ethanol for 15 minutes each and then dried in an oven at 120 °C for an hour. The target complexes were first dissolved in chloroform (*ca*. 10 mg mL^{-1}). Then, the chloroform solutions were spin-coated onto the ITO substrate followed by solvent removal. Aluminium top electrode was deposited onto the organic surface under a pressure of around 5×10^{-6} mbar in a Trovato thermal evaporation system at a rate of 0.1–0.2 nm s^{-1}. A shadow mask was adopted to define the cathode on the substrate. Devices with area of *ca.* 0.25 mm^2 were obtained. Current–voltage (*I*–*V*) characteristics devices were measured with a programmable Keithley model 4200-SCS semiconductor characterization system in a probe station. The electrical measurements were conducted under ambient conditions. The cross section of the resistive memory devices was determined by SEM experiments. The experiments were performed on a Hitachi S-4800 FEG Scanning Electron Microscopy in the Electron Microscope Unit of The University of Hong Kong.

X-Ray Crystal Structure Determination

Single crystals of [Pt(**L1**)(DMSO)Cl], **1**, **2** and **6** suitable for X-ray diffraction studies have been grown by slow diffusion of methyl *tert*-butyl ether vapour into a concentrated dichloromethane solution of the respective complex. The X-ray diffraction data of [Pt(**L1**)(DMSO)Cl], **2** and **6** were collected on the Bruker D8 VENTURE Photon100 CMOS X-Ray Diffractometer by using graphite monochromatized Mo $K\alpha$ radiation (λ = 0.71073 Å). The X-ray diffraction data of complex **1** were collected on the Bruker D8 VENTURE MetalJet Photon II CMOS X-Ray Diffractometer by using graphite monochromatized Ga $K\alpha$ radiation (λ = 1.34318 Å). The images were interpreted and intensities were integrated by using the DENZO program.[2] The structure was solved by direct methods employing the SHELXS-97 program.[2] Full-matrix least-squares refinement on F^2 was used in the structure refinement. The positions of H atoms were calculated based on the riding mode with thermal parameters equal to 1.2 times that of the associated C atoms and participated in the calculation of final R indices. In the final stage of least-squares refinement, all non-hydrogen atoms were refined anisotropically. The crystallographic data for the structural analysis have been deposited with the Cambridge Crystallographic Data Center (CCDC 2405432–2405435).

Materials and Reagents

Tributyltin chloride, 2,4-pentanedione, 2,2,6,6-tetramethyl-3,5-heptanedione, 1,3-diphenyl-1,3-propanedione and potassium *tert*-butoxide were purchased from Aldrich Chemcial Co. 4-Fluoroacetophenone, methyl 4-fluorobenzoate, 4-(trifluoromethyl)acetophenone, methyl 4-(trifluoromethyl)benzoate, 4-phenylacetophenone, methyl 4-phenylbenzoate, 4-hydroxyacetophenone and methyl 4-hydroxybenzoate were purchased from J & K Scientific Ltd. 2-(Tributylstannyl)pyridine,[3] 4-propoxyacetophenone,[4] 4-hexyloxyacetophenone,[4] 4-decyloxyacetophenone,[4] 4-hexadecyloxyacetophenone,[4] methyl 4-propxybenzoate,[5] methyl 4-hexyloxybenzoate,[5] methyl 4-decyloxybenzoate,[5] methyl 4-hexadecyloxybenzoate,[5] [Pt(**L1**)(DMSO)Cl][6] and [Pt(**L2**)(DMSO)Cl][6] were synthesized according to literature procedures with slight modifications. All other commercially available reagents were of analytical grade and were used as received. All solvents were purified and distilled using standard procedures before use. All amines were distilled over sodium hydroxide and stored over sodium hydroxide before use. All reactions were performed under inert and anhydrous conditions using standard Schlenk techniques unless specified otherwise.

Synthesis

4-Phenyl-2-(pyridin-2-yl)-4*H*-phosphindolo[3,2-*b*]thiophene 4-oxide (**L1**)**.** It was prepared according to the procedure for the synthesis of 2,6-bis(6-methylpyridin-2-yl)-4-phenyl-4*H*-phospholo[3,2-*b*:4,5-*b*']dithiophene 4-oxide,[7] except that 2-bromo-4-phenyl-4*H*-phosphindolo[3,2-*b*]thiophene 4-oxide (1.5 g, 4.2 mmol) and 2-(tributylstannyl)pyridine (2.3 g, 6.2 mmol) were used in place of 2,6-dibromo-4-phenyl-4*H*-phosphindolo[3,2-*b*:4,5-*b*']dithiophene 4-oxide and 2-methyl-6-(tributylstannyl)pyridine. Yield: 0.82 g, 2.3 mmol; 55 %. ^{1}H NMR (400 MHz, $CDCl_3$, 298 K, relative to $SiMe_4$, δ/ppm): δ 7.19–7.21 (m, 1H, pyridine), 7.31–7.35 (m, 1H, thienyl), 7.41–7.44 (m, 2H, phenyl), 7.51–7.53 (m, 3H, phenyl), 7.61–7.63 (m, 3H, phenyl and pyridine), 7.70–7.77 (m, 3H, phenyl and thienyl), 8.56 (d, J = 7.9 Hz, 1H, pyridine). ^{31}P{^{1}H} NMR (162 MHz, $CDCl_3$, 298 K, δ/ppm): δ 25.7. Positive ESI-MS: *m/z* 360.06 $[M+H]^+$.

4-Benzo[*b*]thienyl-2-(pyridine-2-yl)-4*H*-phosphindolo[3,2-*b*]thiophene 4-oxide (**L2**)**.** It was prepared according to the procedure for the synthesis of 4-phenyl-2-(pyridin-2-yl)-4*H*-phosphindolo[3,2-*b*]thiophene 4-oxide, except that 2-bromo-4-(benzo[*b*]thienyl)-4*H*-phosphindolo[3,2-*b*]thiophene 4-oxide (1.5 g, 3.6 mmol) was used in place of 2-bromo-4-phenyl-4H-phosphindolo[3,2-b]thiophene 4-oxide. Yield: 0.77 g, 1.9 mmol; 52 %. ^{1}H NMR (400 MHz, $CDCl_3$, 298 K, relative to $SiMe_4$, δ/ppm): δ 7.19–7.21 (m, 1H, pyridine), 7.25–7.37 (m, 2H, phenyl), 7.43–7.46 (m, 2H, phenyl), 7.52–7.57 (m, 1H, phenyl), 7.59–7.64 (m, 2H, phenyl and thienyl), 7.69–7.71 (m, 1H, pyridine), 7.76–7.78 (m, 1H, phenyl), 7.81–7.86 (m, 3H, phenyl) 8.56 (d, J = 7.9 Hz, 1H, pyridine). ^{31}P{^{1}H} NMR (162 MHz, $CDCl_3$, 298 K, δ/ppm): δ 18.9. Positive ESI-MS: *m/z* 416.03 $[M+H]^+$.

General synthetic procedures of complexes 1–10. The complexes were prepared according to a modification of the reported procedures.[6] To a stirred solution of the corresponding platinum(II) precursors and modified 1,3-diketones in tetrahydrofuran (30 mL) was added potassium *tert*-butoxide. The reaction mixture was allowed to reflux for 3 hrs. After removal of solvent, the crude product was purified by slow diffusion of diethyl ether vapor into the concentrated dichloromethane solutions to give the products as yellow or orange solids.

[Pt(L1)(acac)] (acac = 2,4-pentanedione) (**1**)**.** This was synthesized from [Pt(**L1**)(DMSO)Cl] (150 mg, 0.22 mmol), 2,4-pentanedione (27 mg. 0.27 mmol) and potassium *tert*-butoxide (28 mg, 0.25 mmol). Complex **1** was obtained as a yellow solid. Yield: 100 mg, 0.15 mmol; 68 %. ^{1}H NMR (400 MHz, $CDCl_3$, 298 K, relative to $SiMe_4$, δ/ppm): δ 1.59 (s, 3H, $-CH_3$), 1.94 (s, 3H, $-CH_3$), 5.33 (s, 1H, acac-H), 6.96–7.00 (m, 1H, phenyl), 7.26–7.27 (m, 1H, phenyl), 7.33–7.43 (m, 6H, phenyl and pyridine), 7.67–7.76 (m, 2H, phenyl), 7.87–7.93 (m, 2H, phenyl), 8.85 (d, J = 5.5 Hz, 1H, pyridine). ^{31}P{^{1}H} NMR (162 MHz, $CDCl_3$, 298 K, δ/ppm): δ 25.1. HRMS (Positive ESI): calcd for $C_{26}H_{21}NO_3PSPt$, *m/z* 653.0585; found:653.0625 $[M+H]^+$. Elemental analysis calcd (%) for $C_{26}H_{20}NO_3PSPt$: C, 47.85; H, 3.09; N, 2.15; found: C, 47.81; H, 3.07; N, 1.95.

[Pt(L1)(dbm)] (dbm = 1,3-diphenyl-1,3-propanedione) (**2**)**.** This was synthesized from [Pt(**L1**)(DMSO)Cl] (150 mg, 0.22 mmol), 1,3-diphenyl-1,3-propanedione (62 mg. 0.27 mmol) and potassium *tert*-butoxide (28 mg, 0.25 mmol). Complex **2** was obtained as a yellow solid. Yield: 85 mg, 0.11 mmol; 49 %. ^{1}H NMR (400 MHz, $CDCl_3$, 298 K, relative to $SiMe_4$, δ/ppm): δ 6.48 (s, 1H, acac-H), 6.97–6.98 (m, 2H, pyridine),

7.11–7.13 (m, 1H, pyridine), 7.24–7.26 (m, 1H, phenyl), 7.26–7.27 (m, 1H, phenyl), 7.37–7.43 (m, 3H, phenyl), 7.51–7.61 (m, 3H, phenyl), 7.73–7.74 (m, 2H, phenyl), 7.94 (d, *J* = 8.7 Hz, 2H, phenyl), 8.03 (d, *J* = 8.7 Hz, 2H, phenyl), 9.07 (d, *J* = 5.5 Hz, 1H, pyridine). $^{31}P\{^{1}H\}$ NMR (162 MHz, $CDCl_3$, 298 K, *δ*/ppm): *δ* 25.6. HRMS (Positive ESI): calcd for $C_{36}H_{24}NO_3PSPt$, *m/z* 776.0866; found:776.0860 $[M]^+$. Elemental analysis calcd (%) for $C_{36}H_{24}NO_3PSPt$: C, 55.67; H, 3.11; N, 1.80; found: C, 55.47; H, 3.22; N, 1.66.

[Pt(L1){dbm-((CF_3)-4)$_2$}] ({dbm-((CF_3)-4)$_2$} = 1,3-bis(4-(trifluoromethyl)phenyl)-1,3-propanedione) (**3**)**.** This was synthesized from [Pt(**L1**)(DMSO)Cl] (150 mg, 0.22 mmol), 1,3-bis(4-(trifluoromethyl)phenyl)-1,3-propanedione (97 mg. 0.27 mmol) and potassium *tert*-butoxide (28 mg, 0.25 mmol). Complex **3** was obtained as a yellow solid. Yield: 112 mg, 0.13 mmol; 55 %. ^{1}H NMR (400 MHz, $CDCl_3$, 298 K, relative to $SiMe_4$, *δ*/ppm): *δ* 6.41 (s, 1H, acac-H), 6.95–6.97 (m, 2H, phenyl), 7.08–7.10 (m, 2H, phenyl), 7.27–7.31 (m, 1H, phenyl), 7.38–7.41 (m, 3H, pyridine), 7.57–7.62 (m, 4H, phenyl), 7.62–7.76 (m, 4H, phenyl), 8.03–8.05 (m, 4H, phenyl), 9.02 (d, *J* = 5.5 Hz, 1H, pyridine). $^{31}P\{^{1}H\}$ NMR (162 MHz, $CDCl_3$, 298 K, *δ*/ppm): *δ* 26.0. HRMS (Positive ESI): calcd for $C_{38}H_{23}F_6NO_3PSPt$, *m/z* 913.0686; found:913.0658 $[M+H]^+$. Elemental analysis calcd (%) for $C_{38}H_{22}F_6NO_3PSPt$: C, 50.01; H, 2.43; N, 1.53; found: C, 49.82; H, 2.26; N, 1.51.

[Pt(L1){dbm-(Ph-4)$_2$}] ({dbm-(Ph-4)$_2$} = 1,3-bis([1,1'-biphenyl]-4-yl)-1,3-propanedione) (**4**)**.** This was synthesized from [Pt(**L1**)(DMSO)Cl] (150 mg, 0.22 mmol), 1,3-bis([1,1'-biphenyl]-4-yl)-1,3-propanedione (102 mg. 0.27 mmol) and potassium *tert*-butoxide (28 mg, 0.25 mmol). Complex **4** was obtained as a yellow solid.

Yield: 160 mg, 0.17 mmol; 78 %. ^{1}H NMR (400 MHz, $CDCl_3$, 298 K, relative to $SiMe_4$, δ/ppm): δ 6.59 (s, 1H, acac-H), 6.96–6.99 (m, 2H, phenyl), 7.09–7.11 (m, 2H, phenyl), 7.41–7.51 (m, 10H, pyridine and phenyl), 7.62–7.73 (m, 11H, phenyl), 7.78–7.81 (m, 1H, phenyl), 8.05–8.10 (m, 4H, phenyl), 9.13 (d, J = 5.5 Hz, 1H, pyridine). ^{31}P{^{1}H} NMR (162 MHz, $CDCl_3$, 298 K, δ/ppm): δ 25.9. HRMS (Positive ESI): calcd for $C_{48}H_{33}NO_3PSPt$, *m/z* 929.1565; found: 929.1524 $[M+H]^+$. Elemental analysis calcd (%) for $C_{48}H_{32}NO_3PSPt{\bullet}CH_2Cl_2$: C, 58.05; H, 3.38; N, 1.38; found: C, 57.77; H, 3.44; N, 1.27.

[Pt(L1){dbm-((OC$_3$H$_7$)-4)$_2$}] ({dbm-((OC$_3$H$_7$)-4)$_2$} = 1,3-bis(4-propoxyphenyl)-1,3-propanedione) (**5**)**.** This was synthesized from [Pt(**L1**)(DMSO)Cl] (150 mg, 0.22 mmol), 1,3-bis(4-propoxyphenyl)-1,3-propanedione (92 mg. 0.27 mmol) and potassium *tert*-butoxide (28 mg, 0.25 mmol). Complex **5** was obtained as a yellow solid. Yield: 100 mg, 0.11 mmol; 50 %. ^{1}H NMR (400 MHz, $CDCl_3$, 298 K, relative to $SiMe_4$, δ/ppm): δ 1.08 (m, 6H, $-CH_3$), 1.83–1.88 (m, 4H, $-CH_2-$), 3.96 (t, J = 6.6 Hz, 2H, $-OCH_2-$), 4.02 (t, J = 6.6 Hz, 2H, $-OCH_2-$), 6.44 (s, 1H, acac-H), 6.87–6.93 (m, 4H, phenyl), 7.00–7.04 (m, 3H, pyridine), 7.14–7.16 (m, 1H, phenyl), 7.28–7.37 (m, 2H, phenyl), 7.40–7.42 (m, 2H, phenyl), 7.67–7.74 (m, 4H, phenyl), 7.91 (d, J = 8.7 Hz, 2H, phenyl), 8.03 (d, J = 8.7 Hz, 2H, phenyl), 9.11 (d, J = 5.5 Hz, 1H, pyridine). ^{31}P{^{1}H} NMR (162 MHz, $CDCl_3$, 298 K, δ/ppm): δ 25.8. HRMS (Positive ESI): calcd for $C_{42}H_{36}NO_5PSPt$, *m/z* 893.1776; found: 893.1739 $[M+H]^+$. Elemental analysis calcd (%) for $C_{42}H_{36}NO_5PSPt$: C, 56.50; H, 4.06; N, 1.57; found: C, 56.34; H, 4.05; N, 1.56.

[Pt(L1){dbm-((OC$_6$H$_{13}$)-4)$_2$}] ({dbm-((OC$_6$H$_{13}$)-4)$_2$} = 1,3-bis(4-hexyloxyphenyl)-1,3-propanedione) (**6**)**.** This was synthesized from [Pt(**L1**)(DMSO)Cl] (150 mg, 0.22

mmol), 1,3-bis(4-hexyloxyphenyl)-1,3-propanedione (115 mg. 0.27 mmol) and potassium *tert*-butoxide (28 mg, 0.25 mmol). Complex **6** was obtained as a yellow solid. Yield: 90 mg, 0.01 mmol; 41 %. ^{1}H NMR (400 MHz, $CDCl_3$, 298 K, relative to $SiMe_4$, δ/ppm): δ 0.93 (m, 6H, $-CH_3$), 1.34–1.41 (m, 8H, $-CH_2-$), 1.46–1.63 (m, 4H, $-CH_2-$), 1.77–1.86 (m, 4H, $-CH_2-$), 3.97 (t, J = 6.6 Hz, 2H, $-OCH_2-$), 4.05 (t, J = 6.6 Hz, 2H, $-OCH_2-$), 6.43 (s, 1H, acac-H), 6.87–6.93 (m, 4H, phenyl), 7.00–7.04 (m, 3H, pyridine), 7.15–7.16 (m, 1H, phenyl), 7.27–7.34 (m, 2H, phenyl), 7.39–7.40 (m, 2H, phenyl), 7.67–7.74 (m, 4H, phenyl), 7.90 (d, J = 8.7 Hz, 2H, phenyl), 8.03 (d, J = 8.7 Hz, 2H, phenyl), 9.10 (d, J = 5.5 Hz, 1H, pyridine). ^{31}P{^{1}H} NMR (162 MHz, $CDCl_3$, 298 K, δ/ppm): δ 25.9. HRMS (Positive ESI): calcd for $C_{48}H_{49}NO_5PSPt$, *m/z* 977.2716; found: 977.2675 $[M+H]^+$. Elemental analysis calcd (%) for $C_{48}H_{48}NO_5PSPt{\bullet}H_2O$: C, 57.94; H, 5.06; N, 1.41; found: C, 58.04; H, 4.88; N, 1.50.

[Pt(L1){dbm-((OC$_{10}$H$_{21}$)-4)$_2$}] ({dbm-((OC$_{10}$H$_{21}$)-4)$_2$} = 1,3-bis(4-decyloxyphenyl)-1,3-propanedione) (**7**)**.** This was synthesized from [Pt(**L1**)(DMSO)Cl] (150 mg, 0.22 mmol), 1,3-bis(4-decyloxyphenyl)-1,3-propanedione (145 mg. 0.27 mmol) and potassium *tert*-butoxide (28 mg, 0.25 mmol). Complex **7** was obtained as a yellow solid. Yield: 120 mg, 0.11 mmol; 49 %. ^{1}H NMR (400 MHz, $CDCl_3$, 298 K, relative to $SiMe_4$, δ/ppm): δ 0.88 (t, J = 6.4 Hz, 6H, $-CH_3$), 1.25–1.37 (m, 24H, $-CH_2-$), 1.42–1.52 (m, 4H, $-CH_2-$), 1.77–1.86 (m, 4H, $-CH_2-$), 3.96 (t, J = 6.6 Hz, 2H, $-OCH_2-$), 4.05 (t, J = 6.6 Hz, 2H, $-OCH_2-$), 6.43 (s, 1H, acac-H), 6.80–6.90 (m, 4H, phenyl), 7.00–7.04 (m, 3H, pyridine), 7.13–7.15 (m, 1H, phenyl), 7.30–7.32 (m, 2H, phenyl), 7.38–7.40 (m, 2H, phenyl), 7.65–7.73 (m, 4H, phenyl), 7.90 (d, J = 8.8 Hz, 2H, phenyl), 8.04 (d, J = 8.8 Hz, 2H, phenyl), 9.09 (d, J = 5.6 Hz, 1H, pyridine). ^{31}P{^{1}H} NMR (162 MHz, $CDCl_3$, 298 K, δ/ppm): δ 25.8. HRMS (Positive ESI): calcd for $C_{56}H_{65}NO_5PSPt$, *m/z*

1089.3965; found: 1089.3968 $[M+H]^+$. Elemental analysis calcd (%) for $C_{56}H_{64}NO_5PSPt•CH_2Cl_2$: C, 58.31; H, 5.67; N, 1.19; found: C, 58.21; H, 5.76; N, 1.09.

[Pt(L1){dbm-((OC$_{16}$H$_{33}$)-4)$_2$}] ({dbm-((OC$_{16}$H$_{33}$)-4)$_2$} = 1,3-bis(4-hexadecyl-oxyphenyl)-1,3-propanedione) (**8**)**.** This was synthesized from [Pt(**L1**)(DMSO)Cl] (150 mg, 0.22 mmol), 1,3-bis(4-hexadecyloxyphenyl)-1,3-propanedione (190 mg. 0.27 mmol) and potassium *tert*-butoxide (28 mg, 0.25 mmol). Complex **8** was obtained as a yellow solid. Yield: 140 mg, 0.11 mmol; 50 %. ^{1}H NMR (400 MHz, $CDCl_3$, 298 K, relative to $SiMe_4$, δ/ppm): δ0.88 (t, J = 6.4 Hz, 6H, –CH_3), 1.19–1.26 (m, 48H, –CH_2–), 1.44–1.50 (m, 4H, –CH_2–), 1.78–1.86 (m, 4H, –CH_2–), 3.99 (t, J = 6.6 Hz, 2H, –OCH_2–), 4.05 (t, J = 6.6 Hz, 2H, –OCH_2–), 6.44 (s, 1H, acac-H), 6.87–6.93 (m, 4H, phenyl), 7.00–7.04 (m, 3H, pyridine), 7.14–7.16 (m, 1H, phenyl), 7.28–7.36 (m, 2H, phenyl), 7.40–7.41 (m, 2H, phenyl), 7.67–7.74 (m, 4H, phenyl), 7.91 (d, J = 8.7 Hz, 2H, phenyl), 8.03 (d, J = 8.7 Hz, 2H, phenyl), 9.12 (d, J = 5.6 Hz, 1H, pyridine). ^{31}P{^{1}H} NMR (162 MHz, $CDCl_3$, 298 K, δ/ppm): δ 25.8. HRMS (Positive ESI): calcd for $C_{68}H_{89}NO_5PSPt$, *m/z* 1257.5855; found: 1257.5847 $[M+H]^+$. Elemental analysis calcd (%) for $C_{68}H_{88}NO_5PSPt•CHCl_3$: C, 60.19; H, 6.51; N, 1.02; found: C, 59.88; H, 6.66; N, 1.01.

[Pt(L2)(dbm)] (dbm = 1,3-diphenyl-1,3-propanedione) (**9**)**.** This was synthesized from [Pt(**L2**)(DMSO)Cl] (150 mg, 0.22 mmol), 1,3-diphenyl-1,3-propanedione (62 mg. 0.27 mmol) and potassium *tert*-butoxide (28 mg, 0.25 mmol). Complex **9** was obtained as an orange solid. Yield: 75 mg, 0.09 mmol; 43 %. ^{1}H NMR (400 MHz, $CDCl_3$, 298 K, relative to $SiMe_4$, δ/ppm): δ 6.49 (s, 1H, acac-H), 6.96–7.05 (m, 3H, pyridine), 7.12–7.14 (m, 1H, phenyl), 7.28–7.30 (m, 1H, phenyl), 7.36–7.53 (m, 8H, phenyl),

7.68–7.79 (m, 4H, phenyl), 7.93–8.00 (m, 5H, phenyl), 7.73–7.74 (m, 2H, phenyl), 7.94 (d, *J* = 8.7 Hz, 2H, phenyl), 8.03 (d, *J* = 8.7 Hz, 2H, phenyl), 9.07 (d, *J* = 5.5 Hz, 1H, pyridine). $^{31}P\{^{1}H\}$ NMR (162 MHz, $CDCl_3$, 298 K, *δ*/ppm): *δ* 19.6. HRMS (Positive ESI): calcd for $C_{38}H_{25}NO_3PS_2Pt$, *m/z* 833.0659; found: 833.0621 $[M+H]^+$. Elemental analysis calcd (%) for $C_{38}H_{24}NO_3PS_2Pt{\bullet}CH_2Cl_2$: C, 51.64; H, 2.86; N, 1.53; found: C, 51.84; H, 2.92; N, 1.61.

[Pt(L2){dbm-((OC$_{16}$H$_{33}$)-4)$_2$}] ({dbm-((OC$_{16}$H$_{33}$)-4)$_2$} = 1,3-bis(4-hexadecyl-oxyphenyl)-1,3-propanedione) (**10**)**.** This was synthesized from [Pt(**L2**)(DMSO)Cl] (150 mg, 0.22 mmol), 1,3-bis(4-hexadecyloxyphenyl)-1,3-propanedione (190 mg, 0.27 mmol) and potassium *tert*-butoxide (28 mg, 0.25 mmol). Complex **10** was obtained as an orange solid. Yield: 102 mg, 0.08 mmol; 37 %. ^{1}H NMR (400 MHz, $CDCl_3$, 298 K, relative to $SiMe_4$, *δ*/ppm): *δ*0.88 (t, *J* = 6.4 Hz, 6H, $-CH_3$), 1.20–1.26 (m, 48H, $-CH_2-$), 1.44–1.53 (m, 4H, $-CH_2-$), 1.75–1.88 (m, 4H, $-CH_2-$), 3.99 (t, *J* = 6.6 Hz, 2H, $-OCH_2-$), 4.05 (t, *J* = 6.6 Hz, 2H, $-OCH_2-$), 6.43 (s, 1H, acac-H), 6.87–6.91 (m, 4H, phenyl), 7.01–7.05 (m, 3H, pyridine), 7.14–7.16 (m, 1H, phenyl), 7.29–7.31 (m, 2H, phenyl), 7.40 (d, *J* = 7.2 Hz, 1H, phenyl), 7.63 (d, *J* = 7.2 Hz, 1H, phenyl), 7.77–7.85 (m, 3H, phenyl), 7.91 (d, *J* = 8.7 Hz, 2H, phenyl), 8.03 (d, *J* = 8.7 Hz, 3H, phenyl), 9.11 (d, *J* = 5.6 Hz, 1H, pyridine).$^{31}P\{^{1}H\}$ NMR (162 MHz, $CDCl_3$, 298 K, *δ*/ppm): *δ* 20.1. HRMS (Positive ESI): calcd for $C_{70}H_{89}NO_5PS_2Pt$, *m/z* 1314.5580; found: 1314.5516 $[M+H]^+$. Elemental analysis calcd (%) for $C_{70}H_{88}NO_5PS_2Pt{\bullet}CH_2Cl_2$: C, 60.97; H, 6.49; N, 1.00; found: C, 60.06; H, 6.51; N, 1.04.

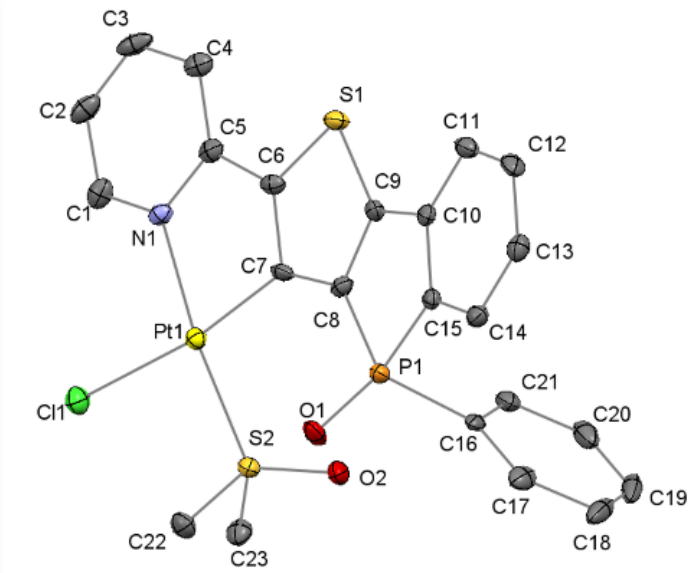

Fig. S1 Perspective view of [Pt(**L1**)(DMSO)Cl] with atomic numbering scheme. Hydrogen atoms have been omitted for clarity. Thermal ellipsoids are shown at the 30 % probability level.

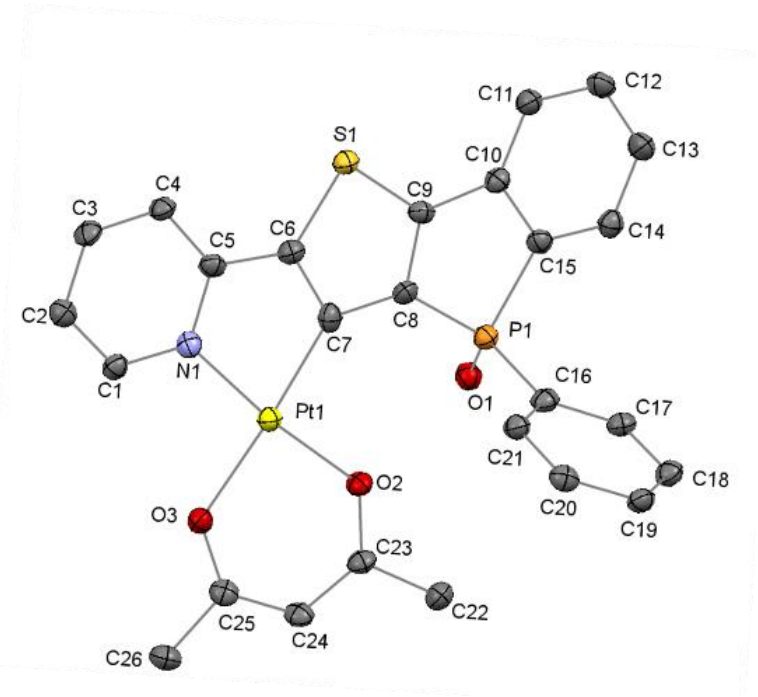

Fig. S2 Perspective view of **1** with atomic numbering scheme. Hydrogen atoms have been omitted for clarity. Thermal ellipsoids are shown at the 30 % probability level.

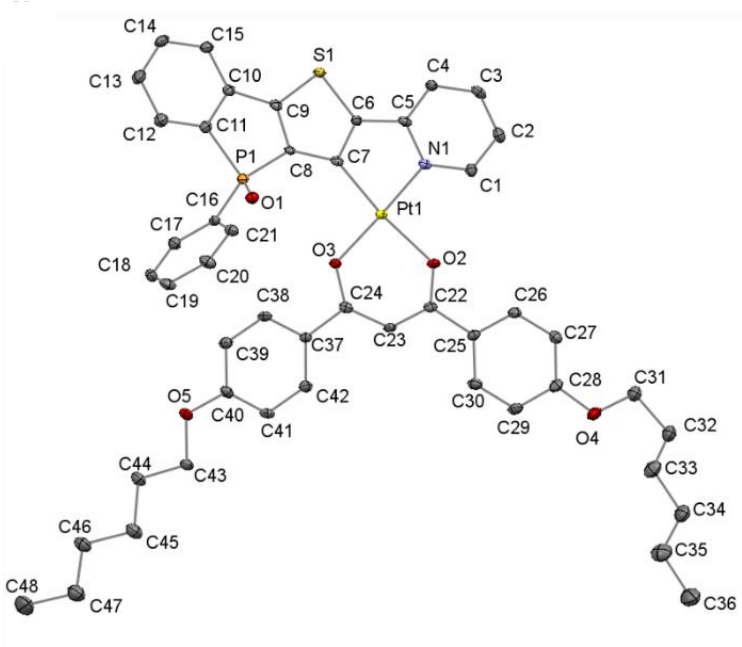

Fig. S3 Perspective view of **6** with atomic numbering scheme. Hydrogen atoms have been omitted for clarity. Thermal ellipsoids are shown at the 30 % probability level.

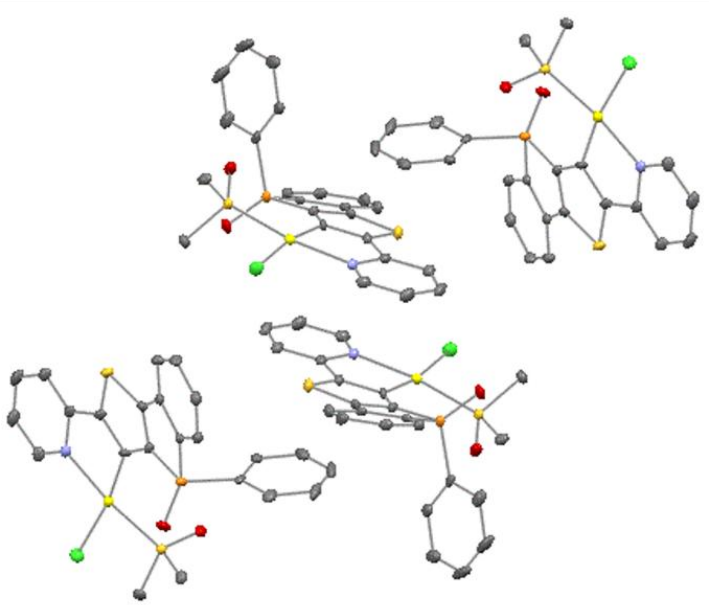

Fig. S4 Crystal packing of [Pt(**L1**)(DMSO)Cl]. Hydrogen atoms have been omitted for clarity. No Pt···Pt interactions are found.

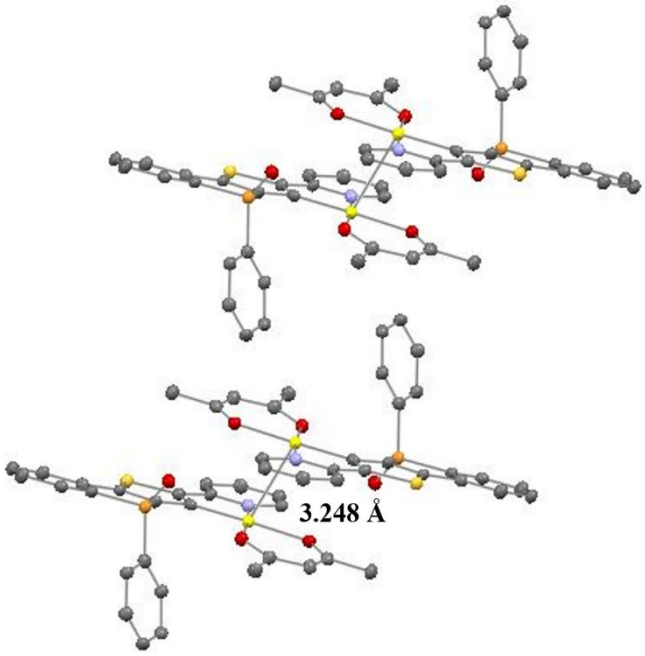

Fig. S5 Crystal packing of **1**. Hydrogen atoms have been omitted for clarity. The Pt···Pt distance is labelled.

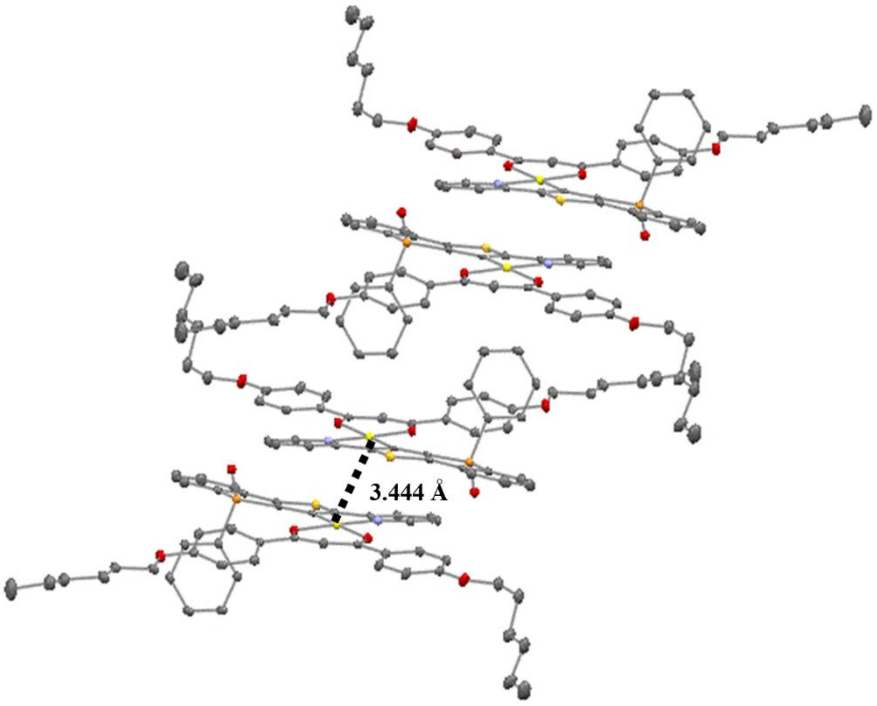

Fig. S6 Crystal packing of **6**. Hydrogen atoms have been omitted for clarity. The Pt···Pt distance is labelled.

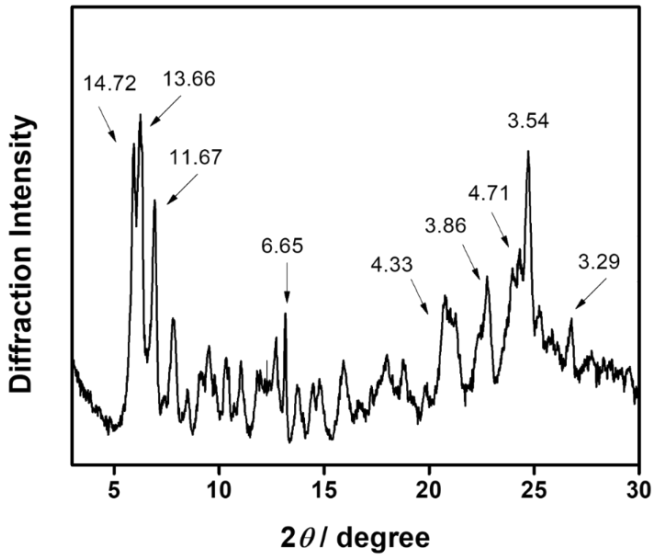

Fig. S7 Powder X-ray diffraction patterns on the solid sample of **5**. Numerical values indicate *d*-spacing (Å).

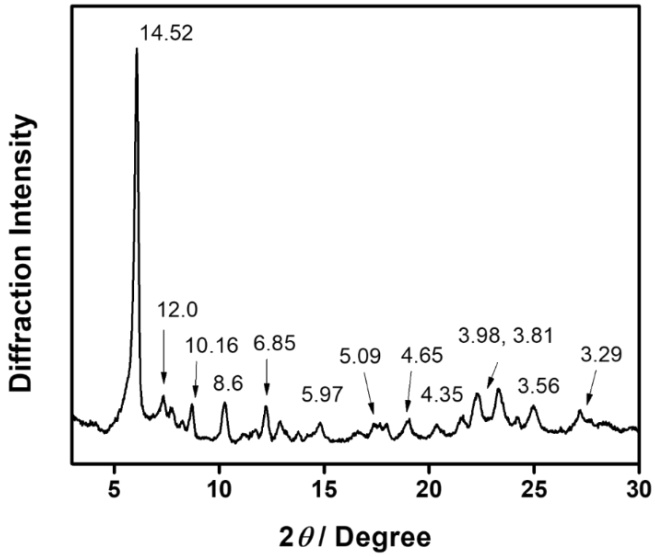

Fig. S8 Powder X-ray diffraction patterns on the solid sample of **6**. Numerical values indicate *d*-spacing (Å).

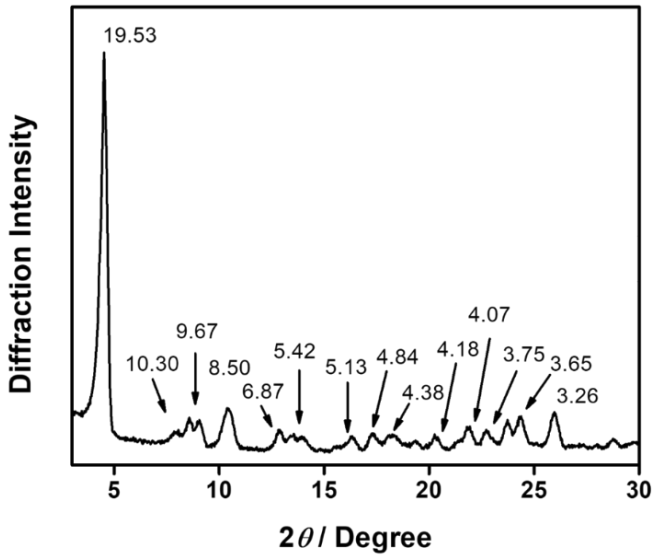

Fig. S9 Powder X-ray diffraction patterns on the solid sample of **7**. Numerical values indicate *d*-spacing (Å).

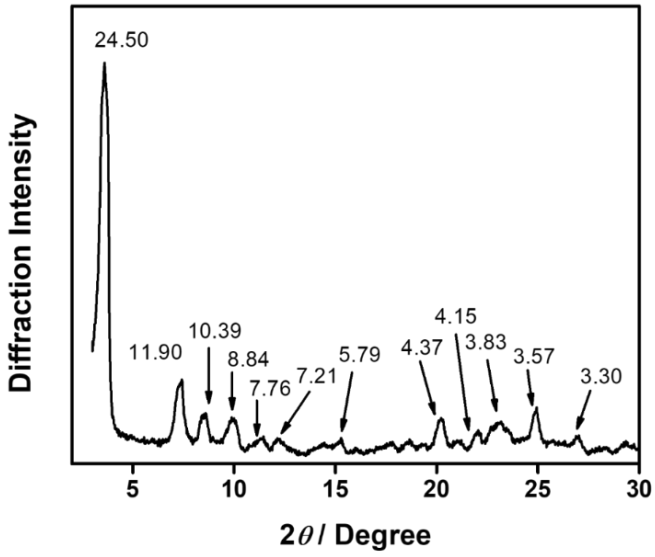

Fig. S10 Powder X-ray diffraction patterns on the solid sample of **8**. Numerical values indicate *d*-spacing (Å).

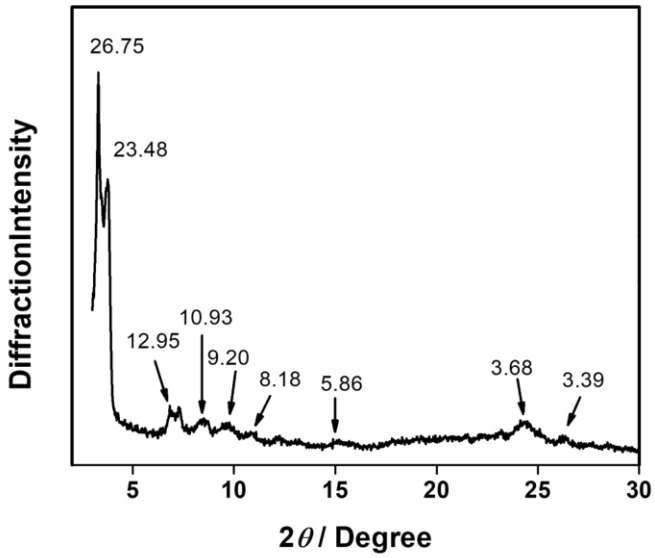

Fig. S11 Powder X-ray diffraction patterns on the solid sample of **10**. Numerical values indicate *d*-spacing (Å).

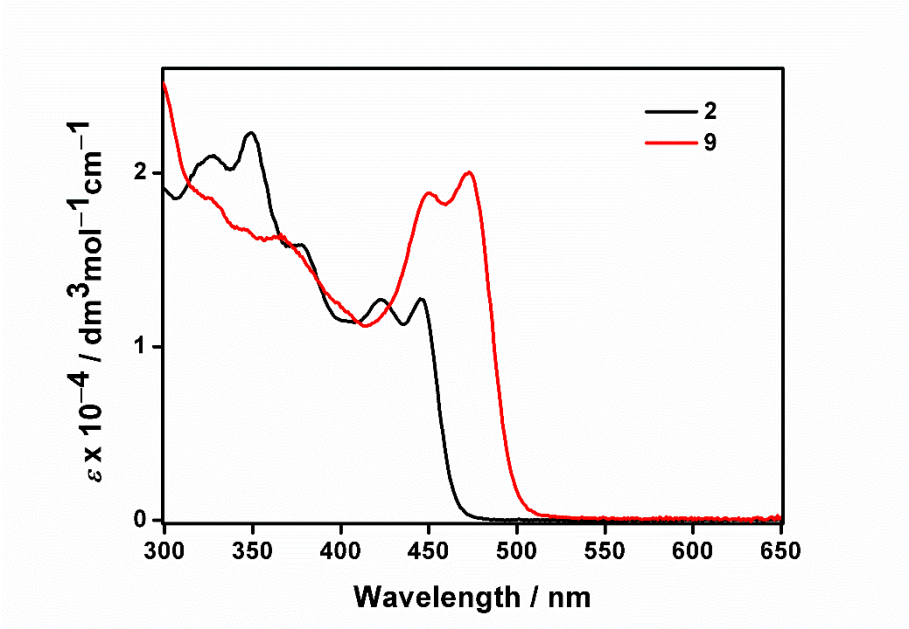

Fig. S12 Electronic absorption spectra of **2** and **9** in dichloromethane solutions at 298 K.

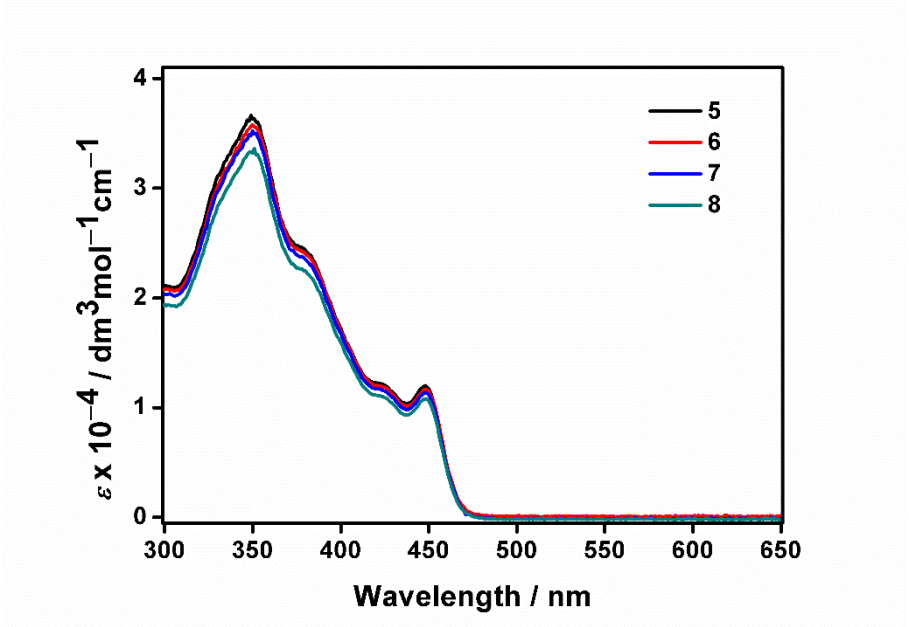

Fig. S13 Electronic absorption spectra of **5–8** in dichloromethane solutions at 298 K.

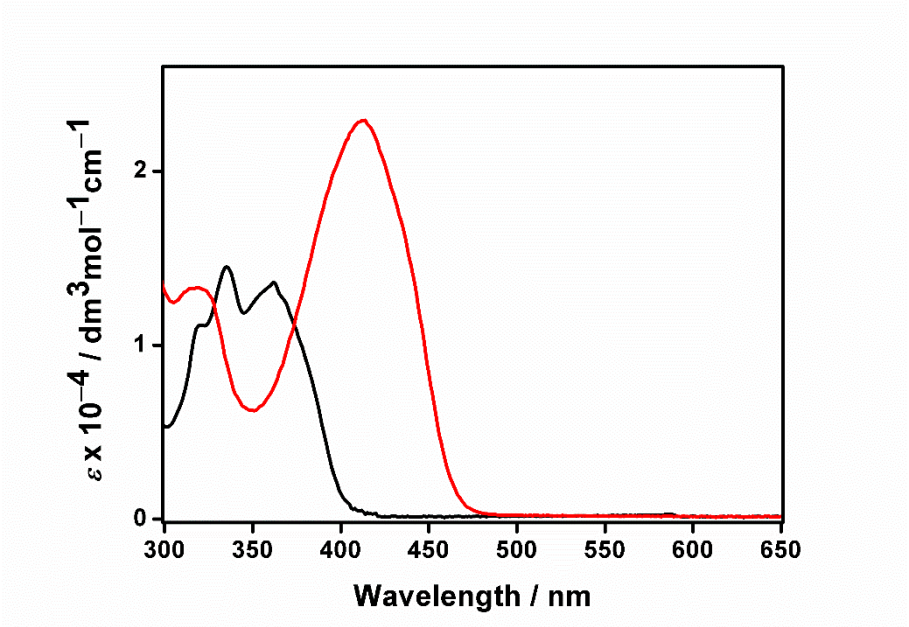

Fig. S14 Electronic absorption spectra of **L1** (black) and **L2** (red) in dichloromethane solutions at 298 K.

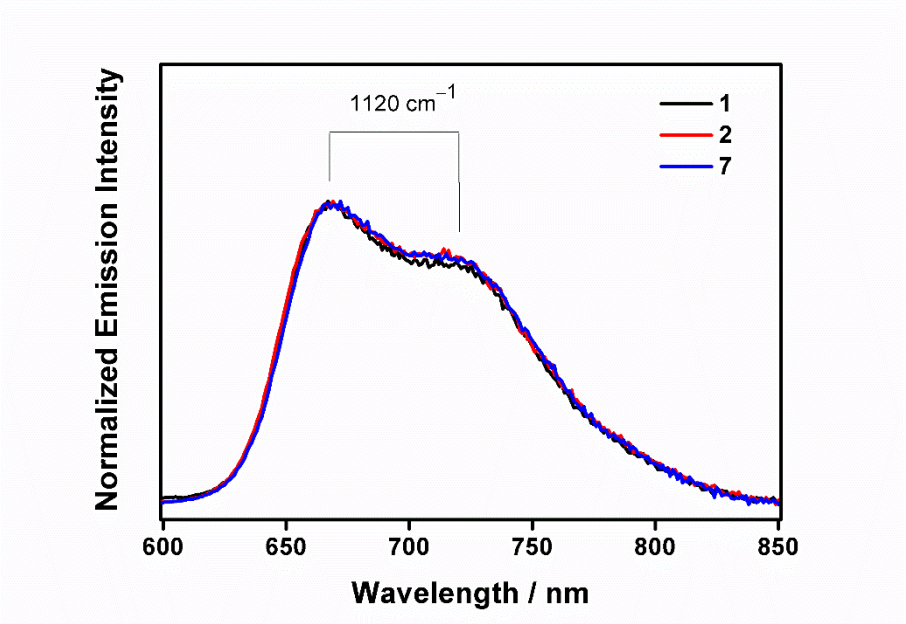

Fig. S15 Normalized emission spectra of **1**, **2** and **7** in degassed dichloromethane solutions at 298 K.

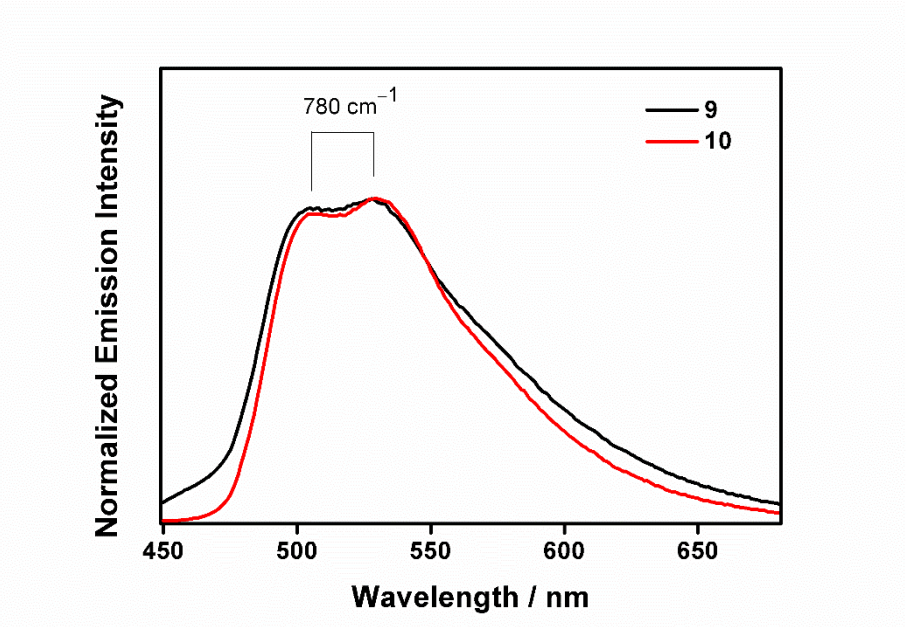

Fig. S16 Normalized emission spectra of **9** and **10** in degassed dichloromethane solutions at 298 K.

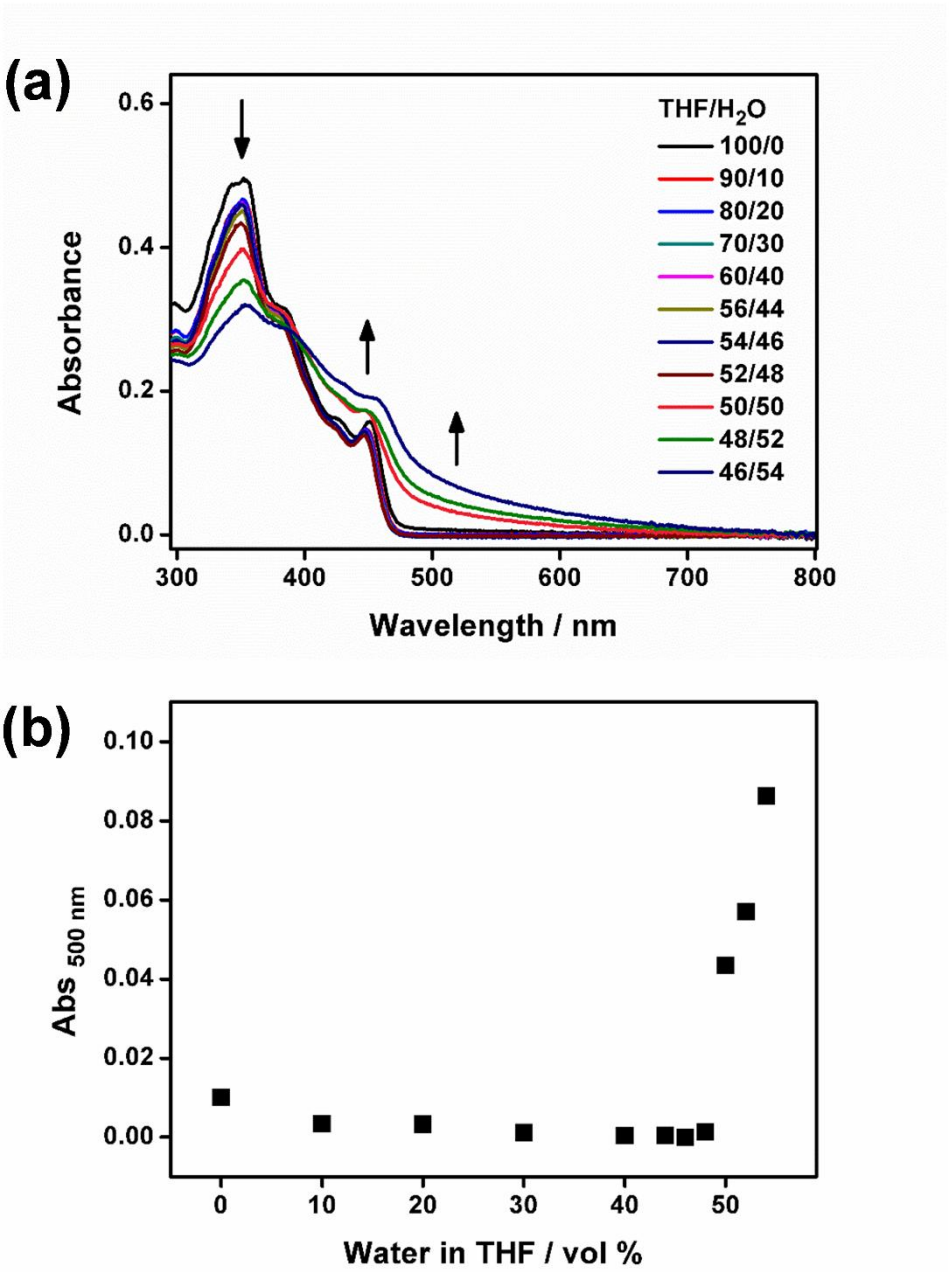

Fig. S17 (a) UV–Vis spectral traces of **8** in THF solutions at 298 K upon increasing the water content from 0 to 50 %. (b) A plot of absorbance at 500 nm as a function of water fraction in the THF solutions of **8**.

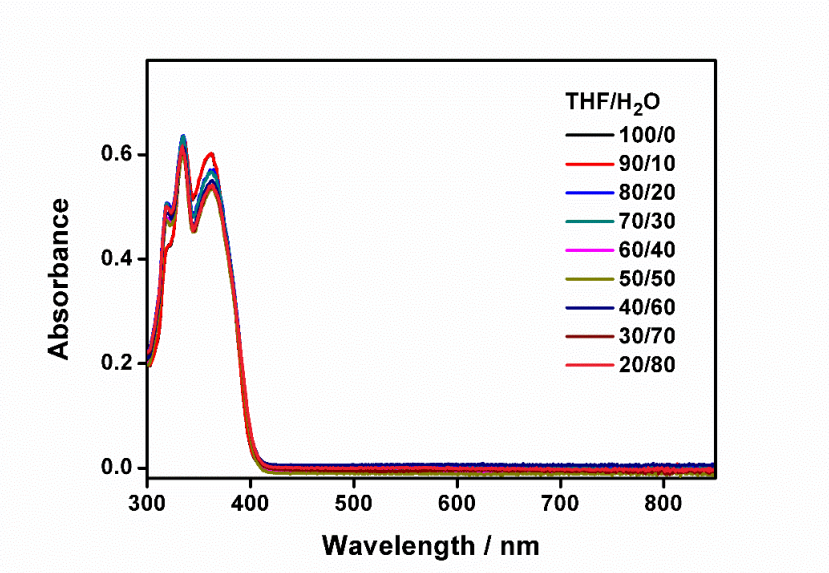

Fig. S18 UV–Vis spectral traces of **L1** in THF solutions at 298 K upon increasing the water content from 0 to 80 %.

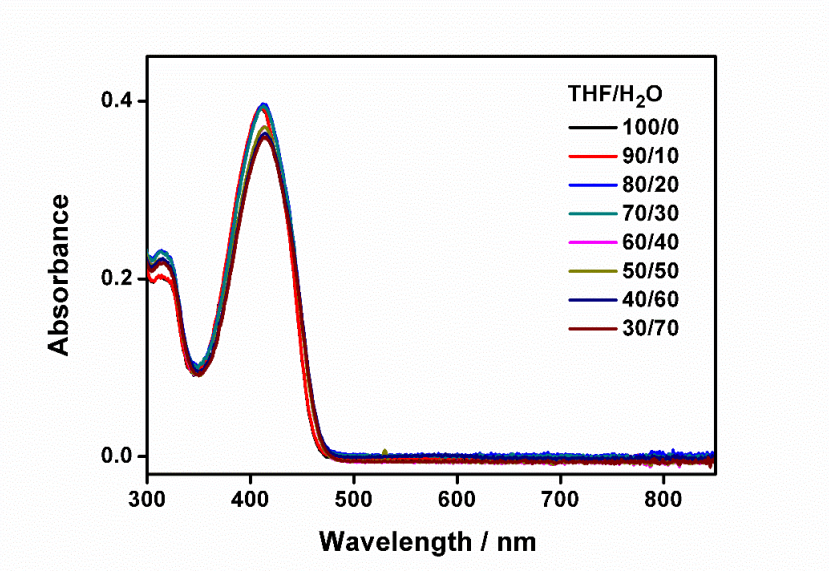

Fig. S19 UV–Vis spectral traces of **L2** in THF solutions at 298 K upon increasing the water content from 0 to 80 %.

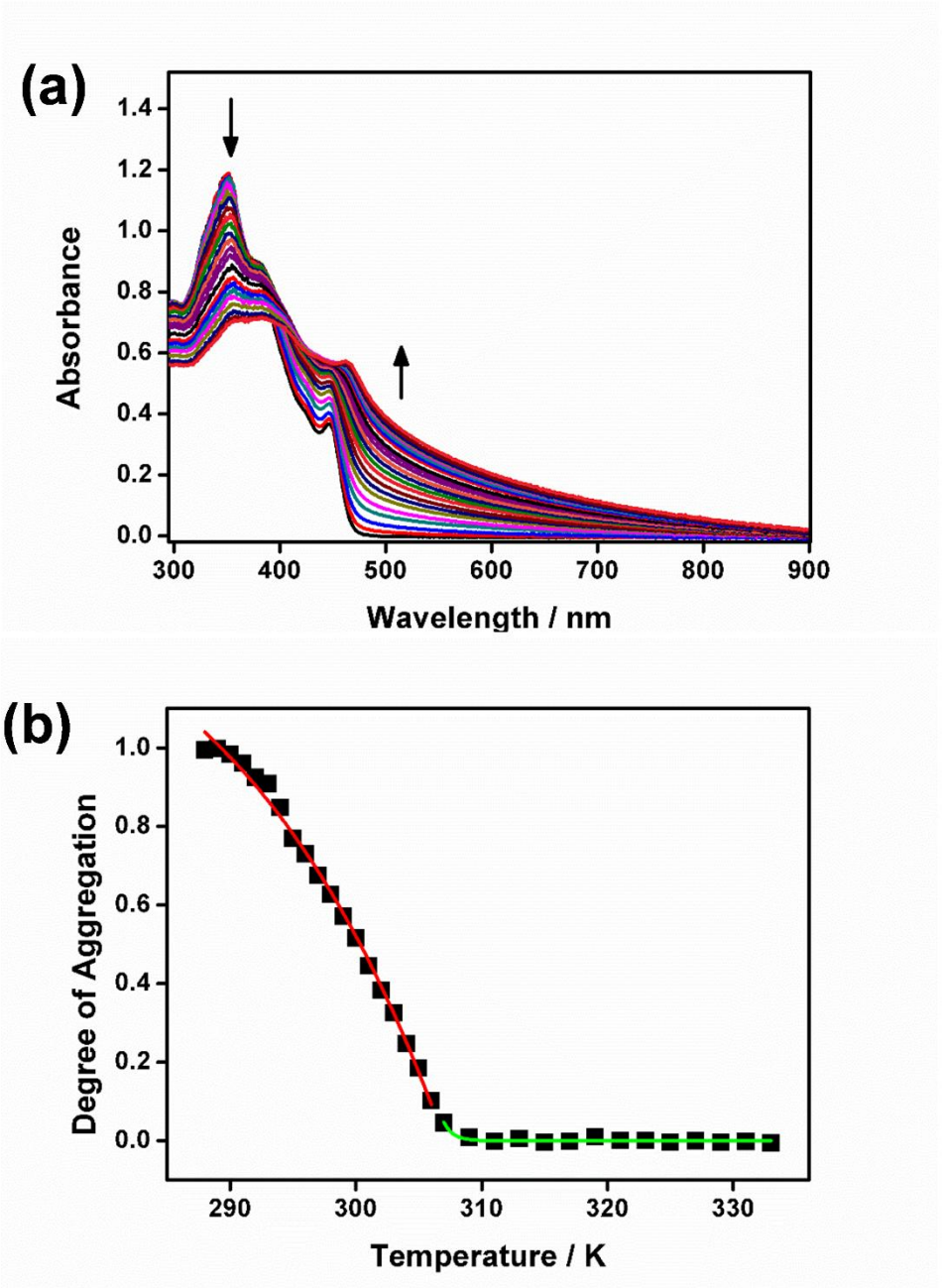

Fig. S20 (a) UV–Vis absorption spectral traces on cooling a solution of **8** in 50 % water–THF mixtures. (b) A plot of the degree of aggregation of **8** as a function of temperature, with the curve fitted at the elongation (red line) and nucleation (green line) regimes.

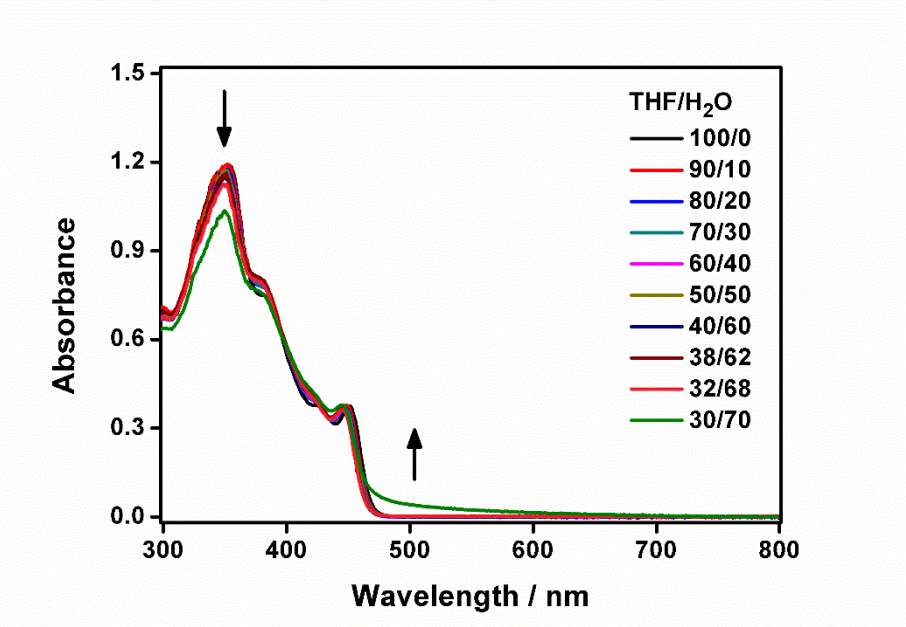

Fig. S21 UV–Vis spectral traces of **5** in THF solutions at 298 K upon increasing the water content from 0 to 70 %.

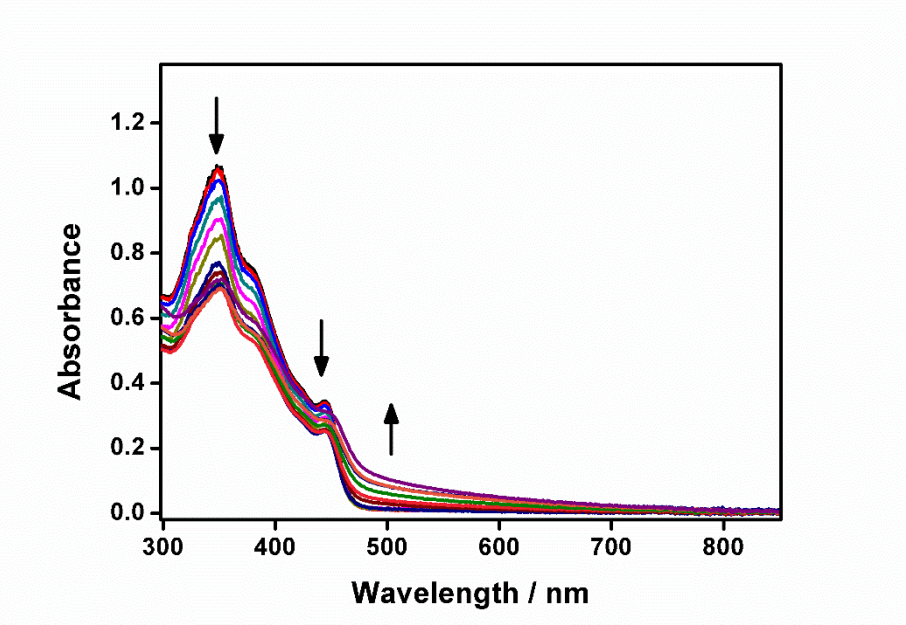

Fig. S22 UV–Vis absorption spectral traces on cooling a solution of **5** in 70 % water–THF mixtures.

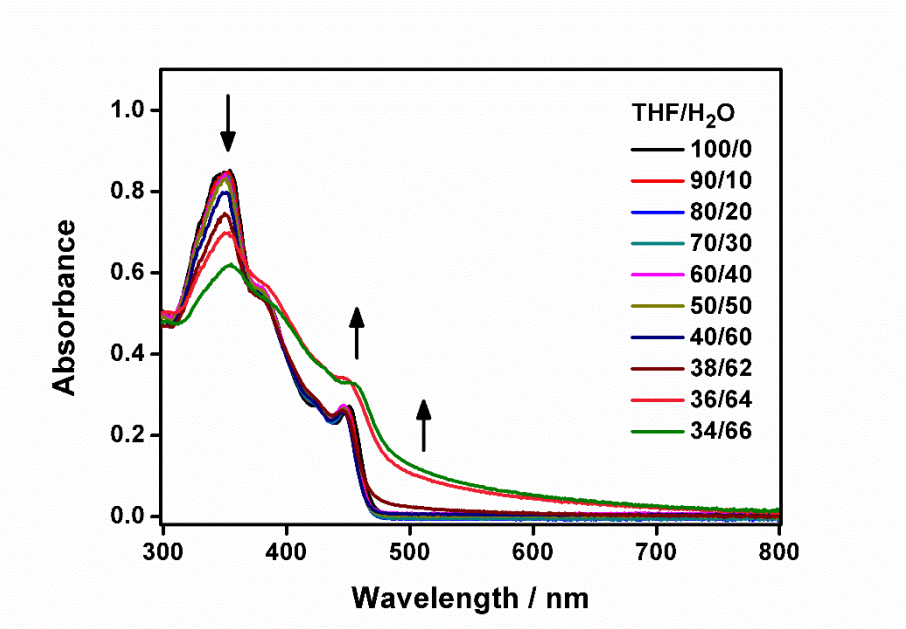

Fig. S23 UV–Vis spectral traces of **6** in THF solutions at 298 K upon increasing the water content from 0 to 66 %.

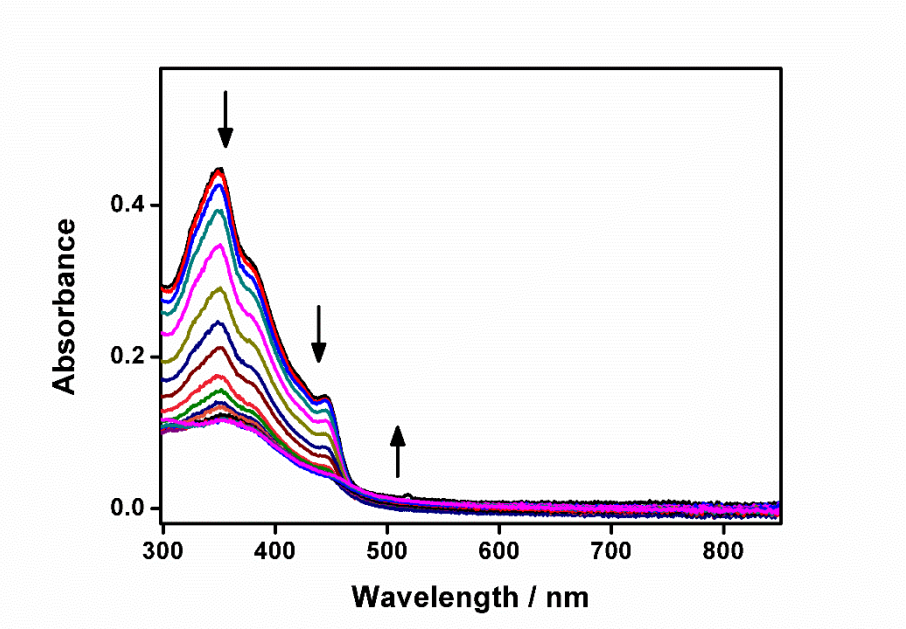

Fig. S24 UV–Vis absorption spectral traces on cooling a solution of **6** in 66 % water–THF mixtures.

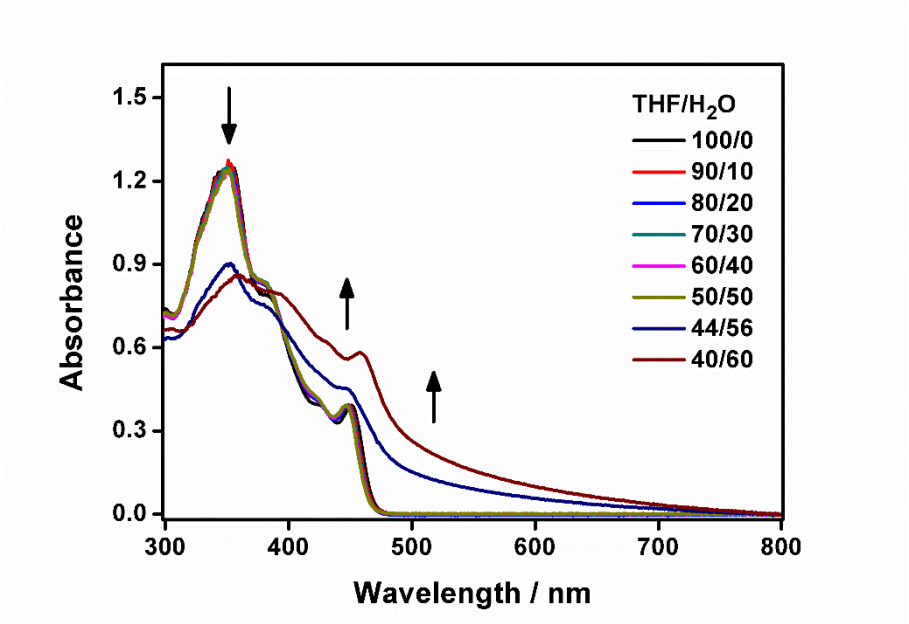

Fig. S25 UV–Vis spectral traces of **7** in THF solutions at 298 K upon increasing the water content from 0 to 60 %.

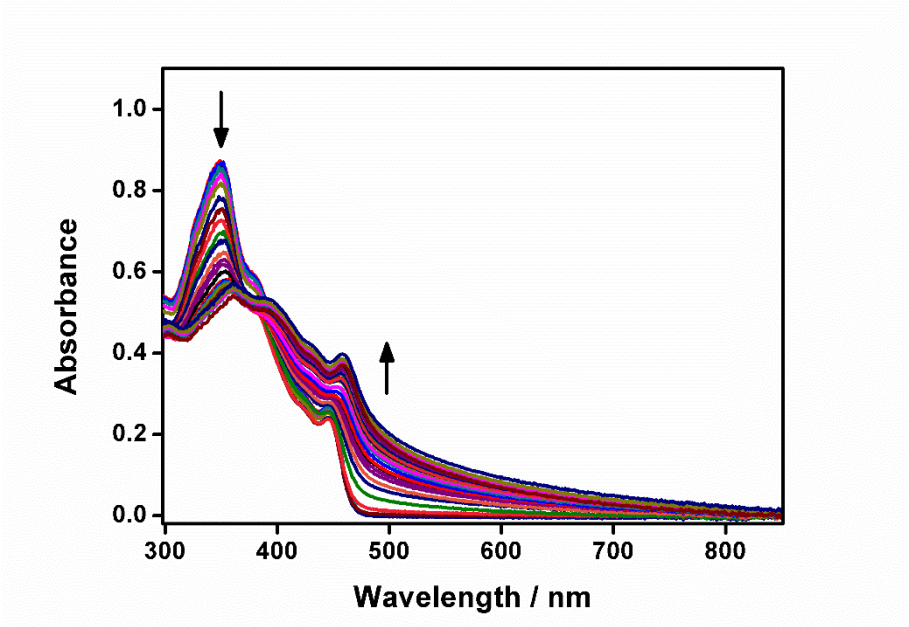

Fig. S26 UV–Vis absorption spectral traces on cooling a solution of **7** in 60 % water–THF mixtures.

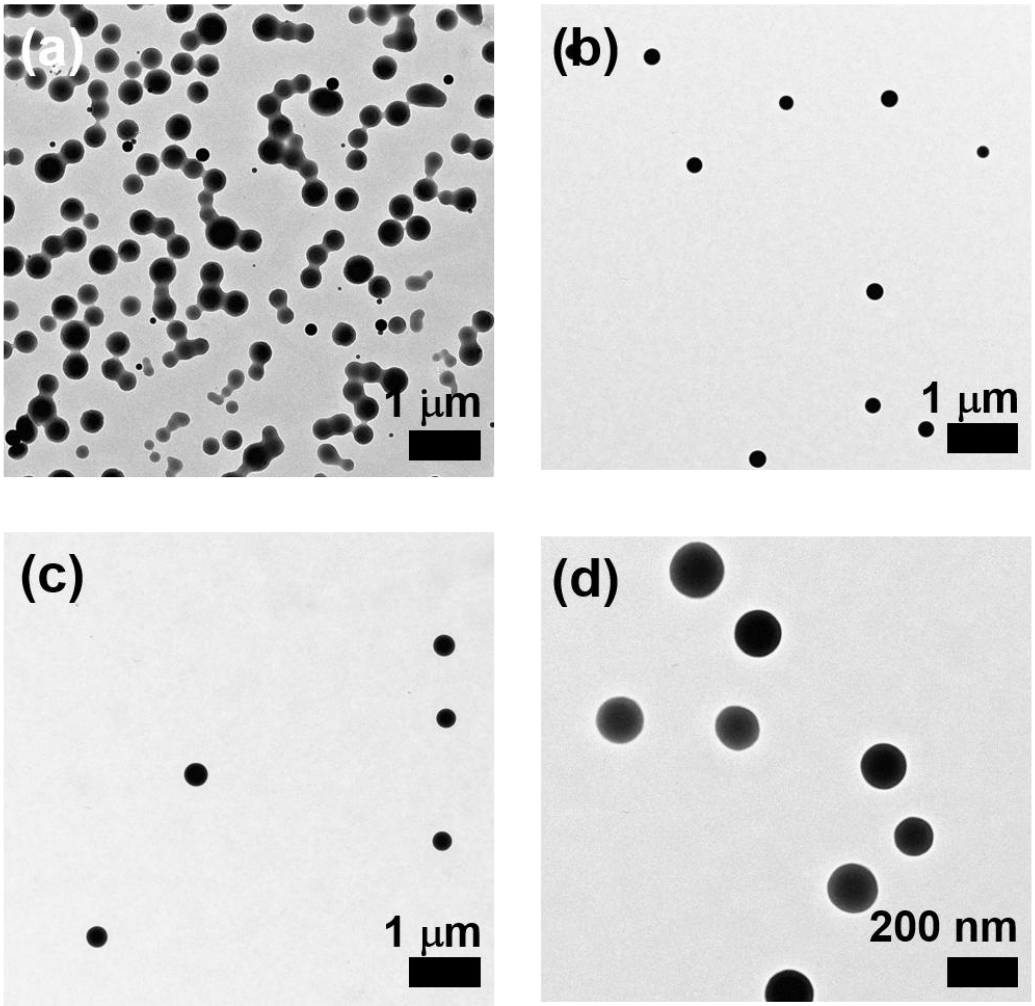

Fig. S27 TEM images of the aggregates prepared from the 50 % water–THF mixture of (a) **5**, (b) **6**, (c) **7**, and (d) **8**.

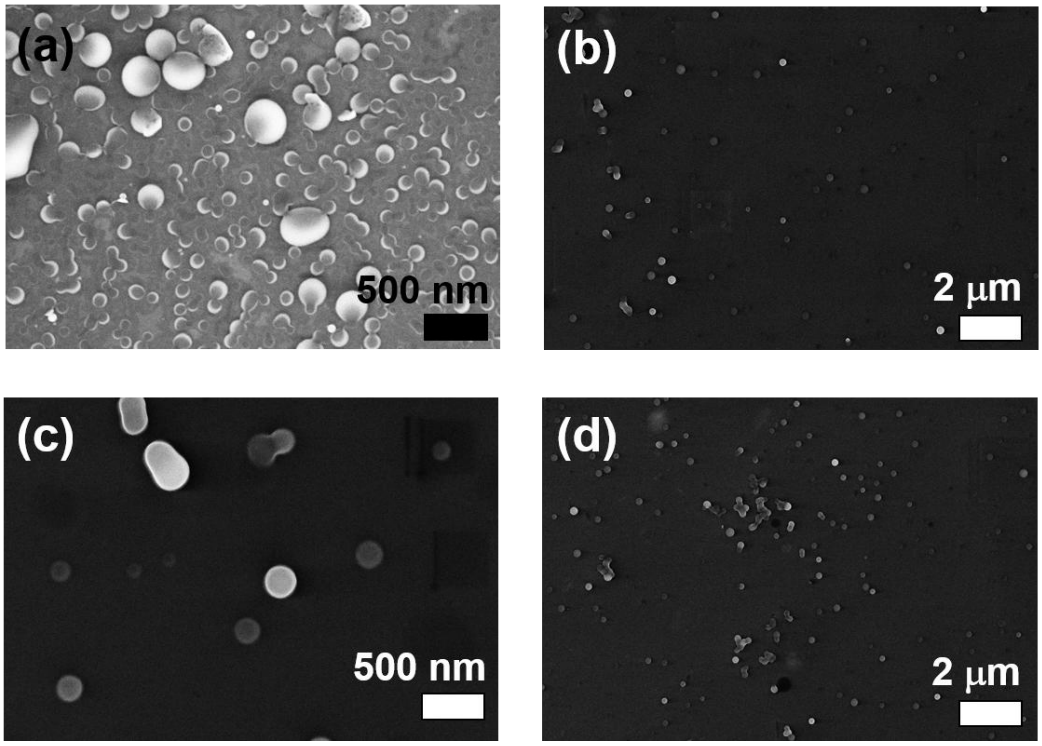

Fig. S28 SEM images of the aggregates prepared from the 50 % water–THF mixture of (a) **5**, (b) **6**, (c) **7**, and (d) **8**.

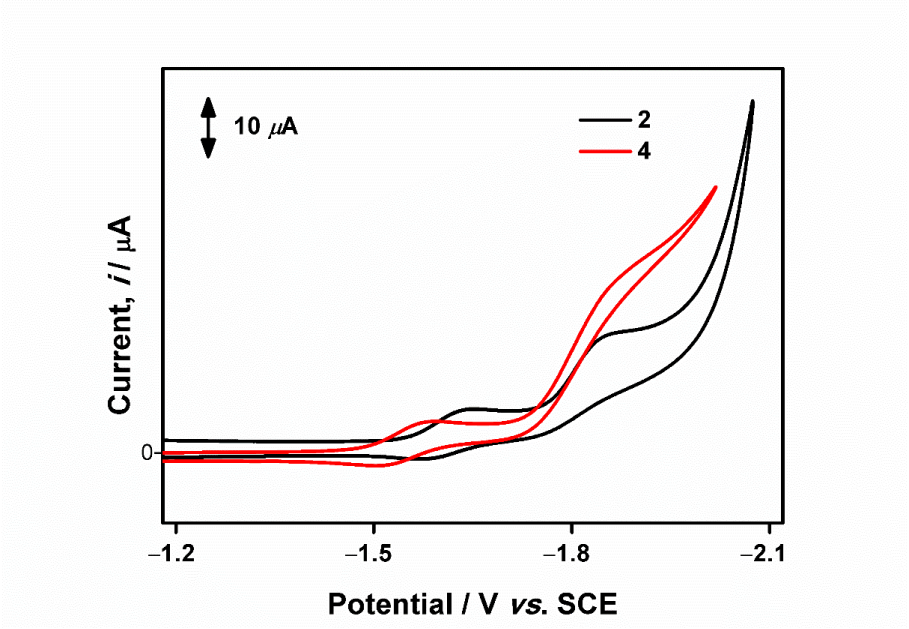

Fig. S29 Cyclic voltammograms for the reductive scan of **2** and **4** in dichloromethane solutions (0.1 M $^{n}Bu_4NPF_6$). Scan rate: 100 mVs^{-1}.

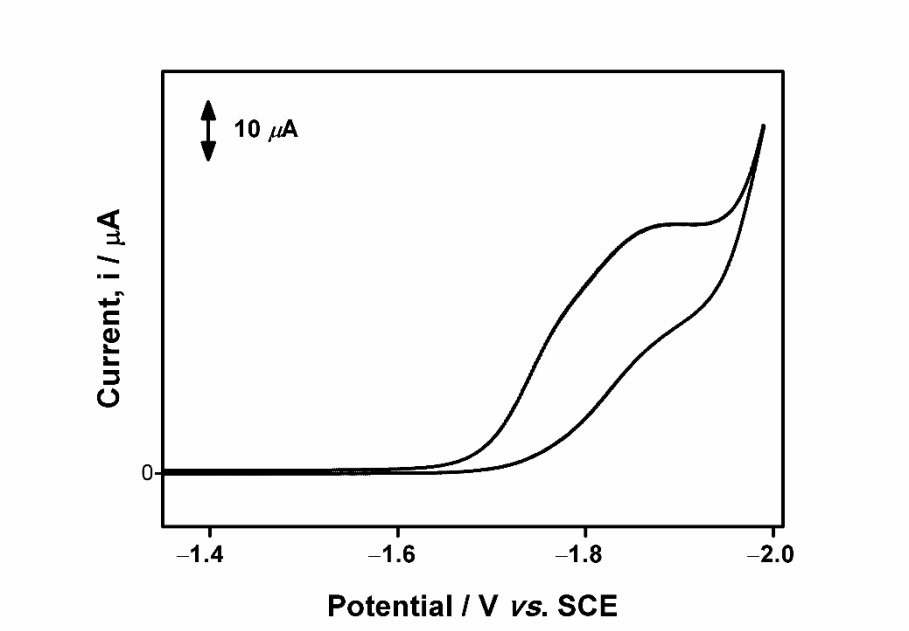

Fig. S30 Cyclic voltammogram for the reductive scans of **L1** in dichloromethane solutions (0.1 M $^{n}Bu_4NPF_6$). Scan rate: 100 mVs^{-1}.

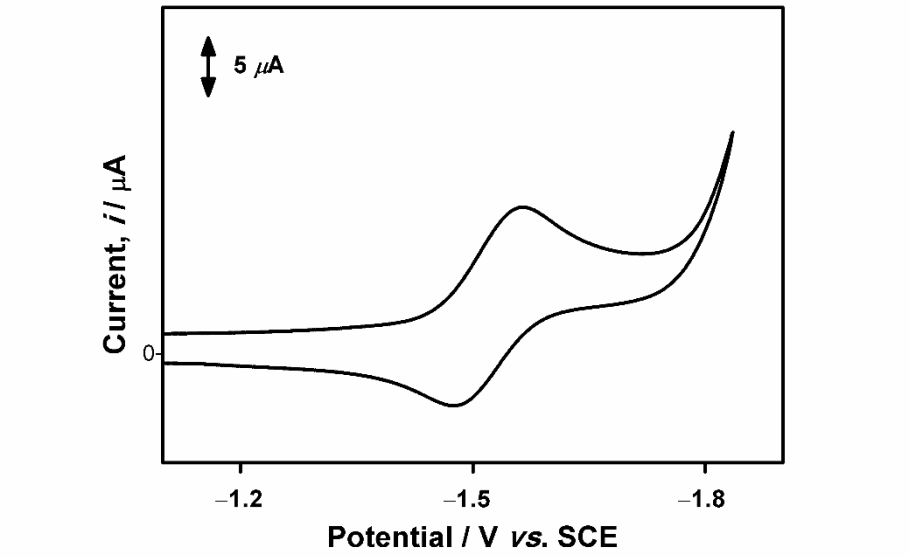

Fig. S31 Cyclic voltammogram for the reductive scan of **L2** in dichloromethane solutions (0.1 M $^{n}Bu_4NPF_6$). Scan rate: 100 mVs^{-1}.

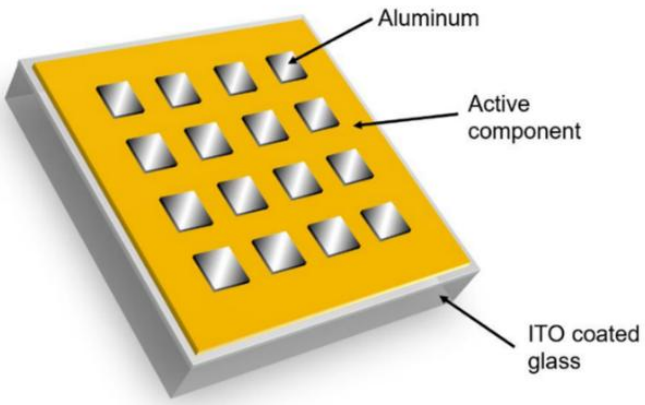

Fig. S32 Schematic structure of a resistive memory device.

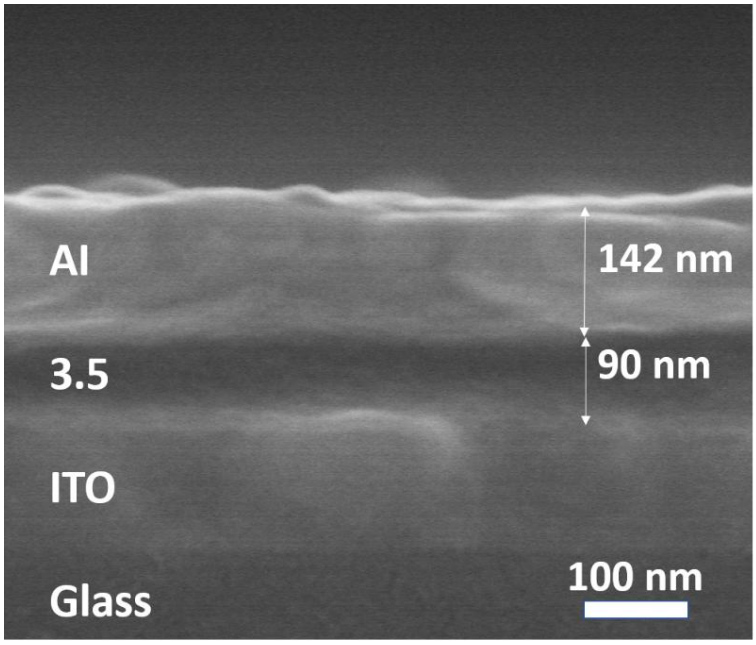

Fig. S33 SEM image of the cross-section of the device fabricated with **3**.

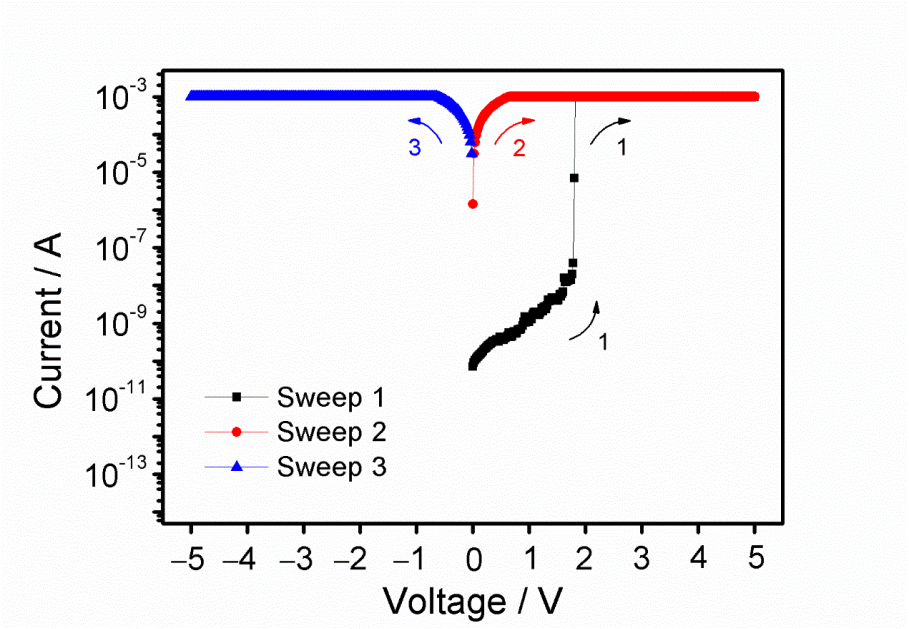

Fig. S34 Current–voltage characteristics of the organic memory device fabricated with **3**.

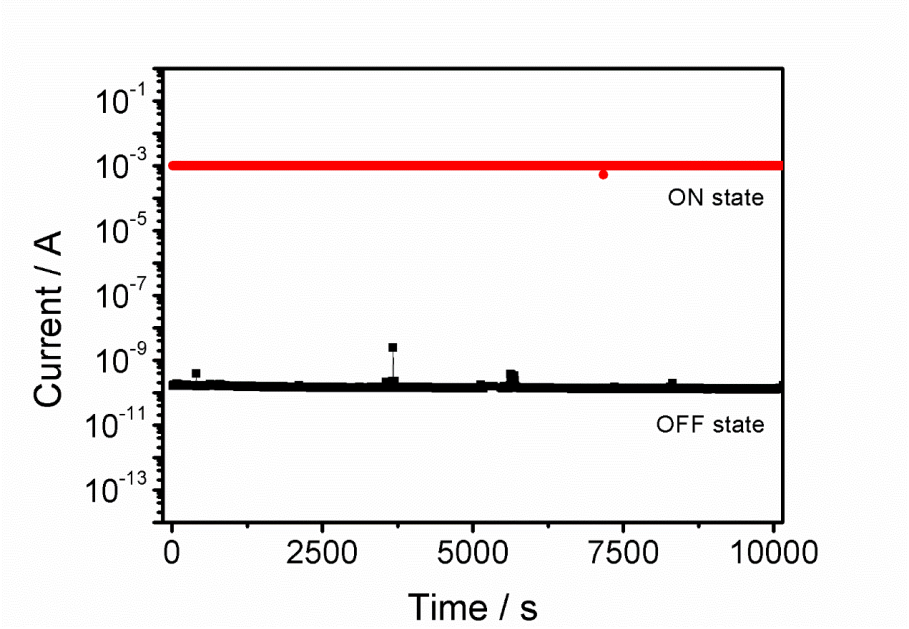

Fig. S35 Stability of the organic memory device **3** in different states under a constant stress at 1 V.

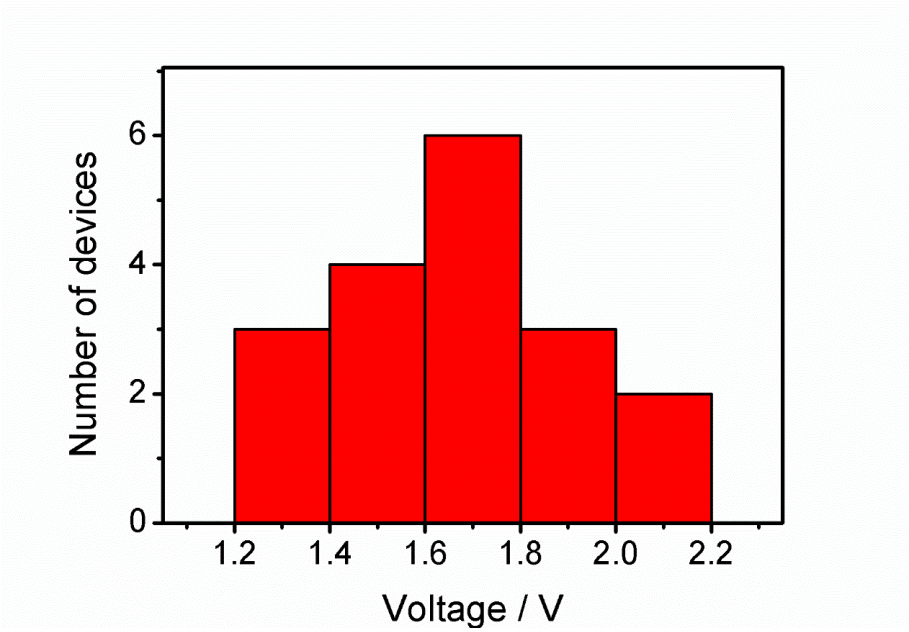

Fig. S36 Distribution of the switching threshold voltages among 20 memory devices fabricated with **3**.

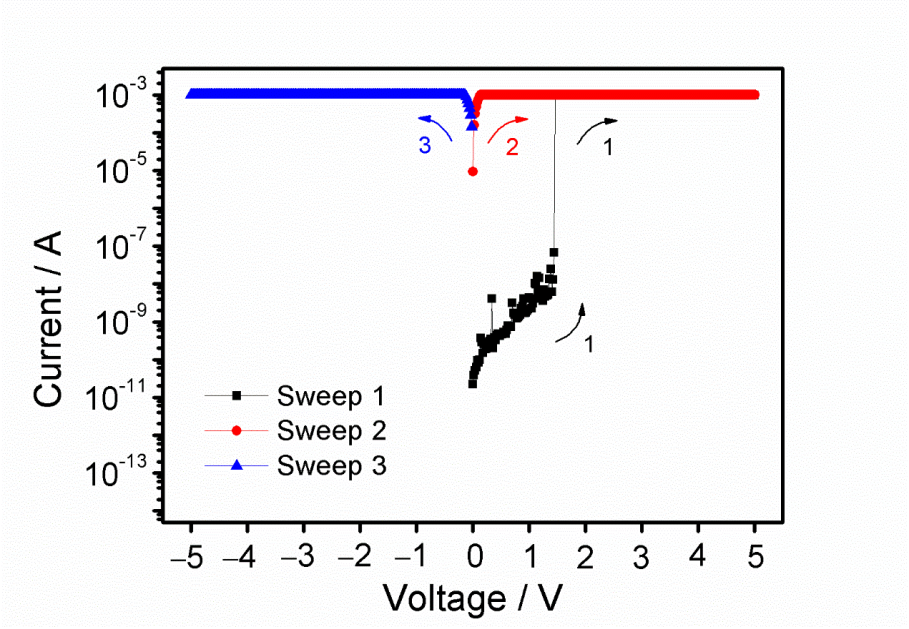

Fig. S37 Current–voltage characteristics of the organic memory device fabricated with **6**.

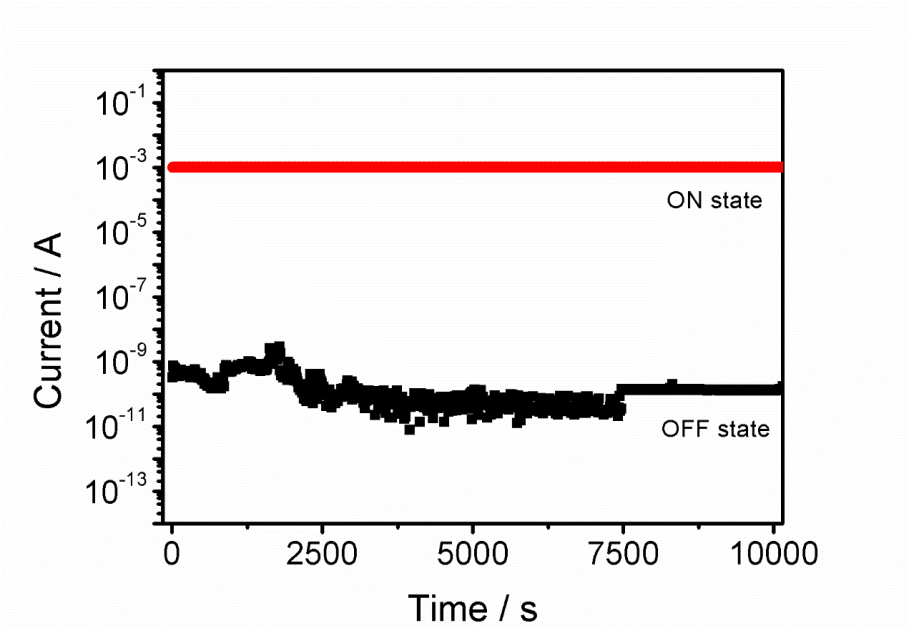

Fig. S38 Stability of the organic memory device fabricated with **6** in different states under a constant stress at 1 V.

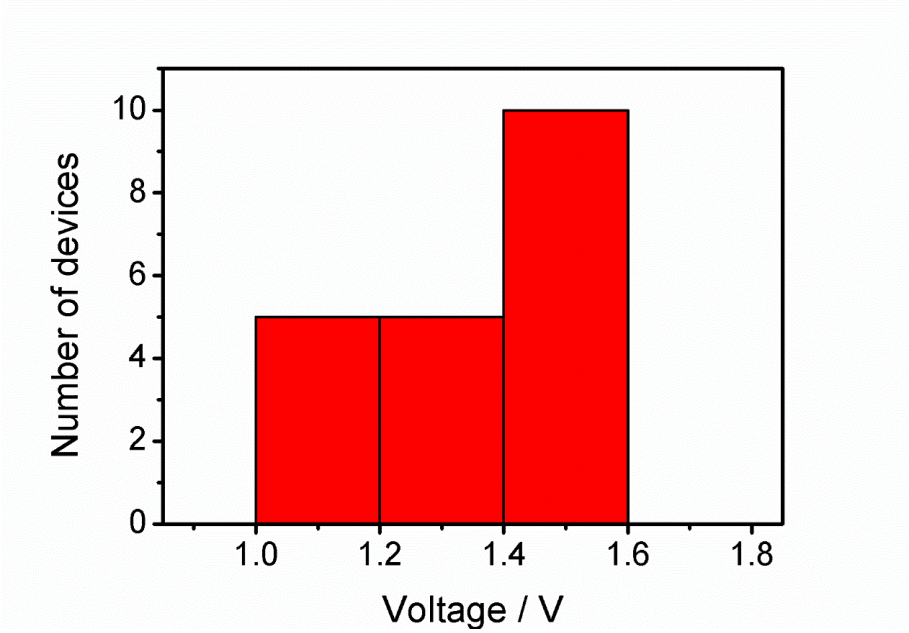

Fig. S39 Distribution of the switching threshold voltages among 20 memory devices fabricated with **6**.

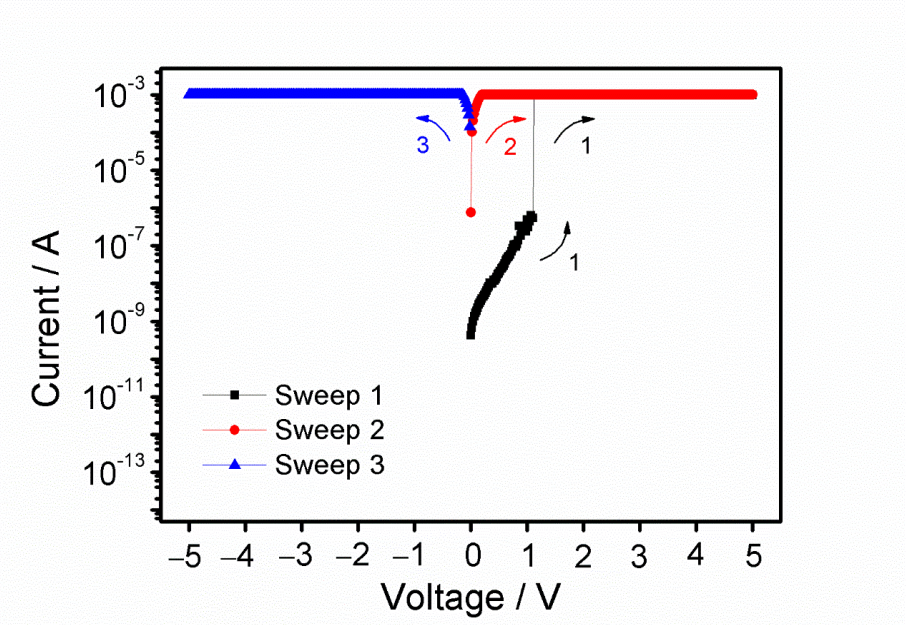

Fig. S40 Current–voltage characteristics of the organic memory device fabricated with **9**.

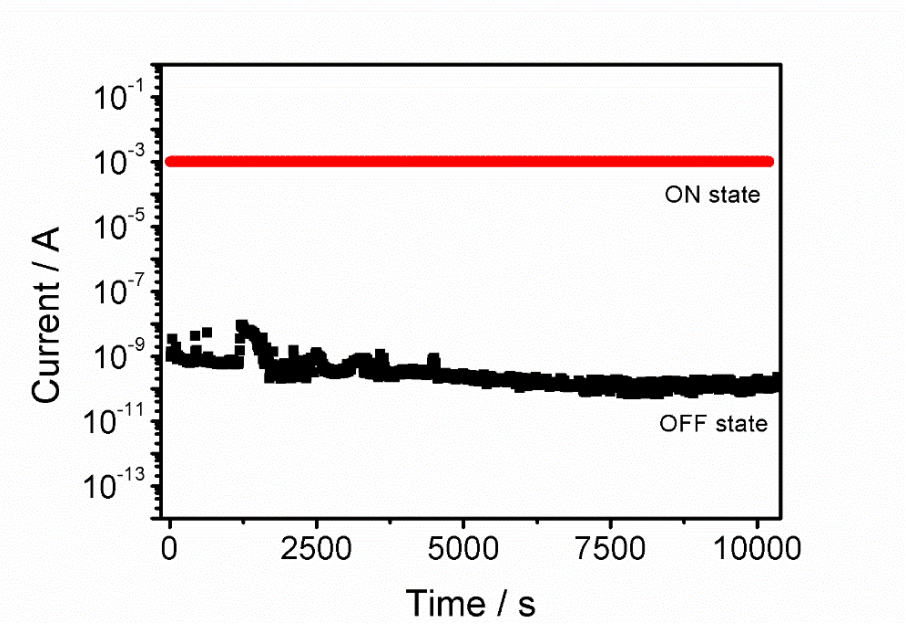

Fig. S41 Stability of the organic memory device fabricated with **9** in different states under a constant stress at 1 V.

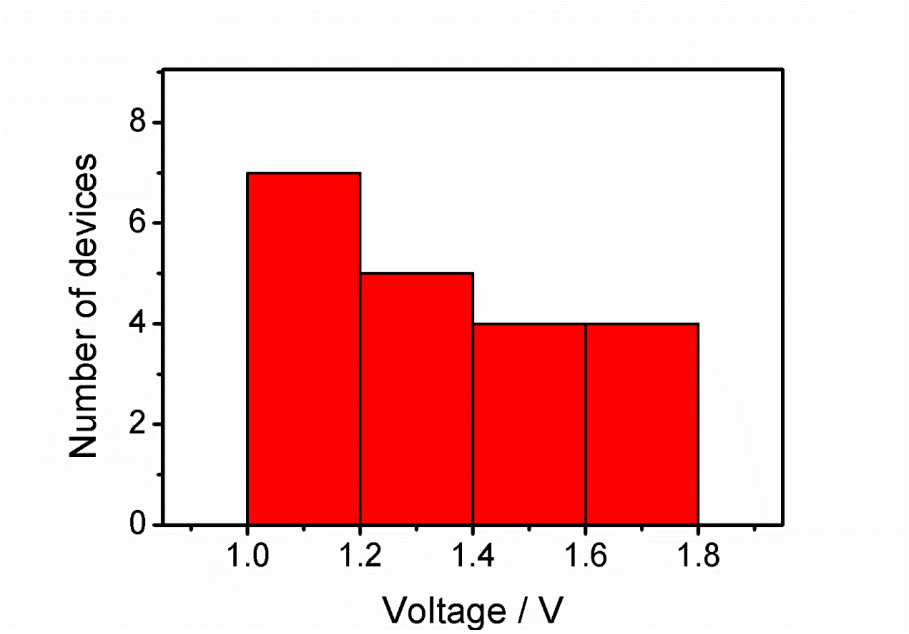

Fig. S42 Distribution of the switching threshold voltages among 20 memory devices fabricated with **9**.

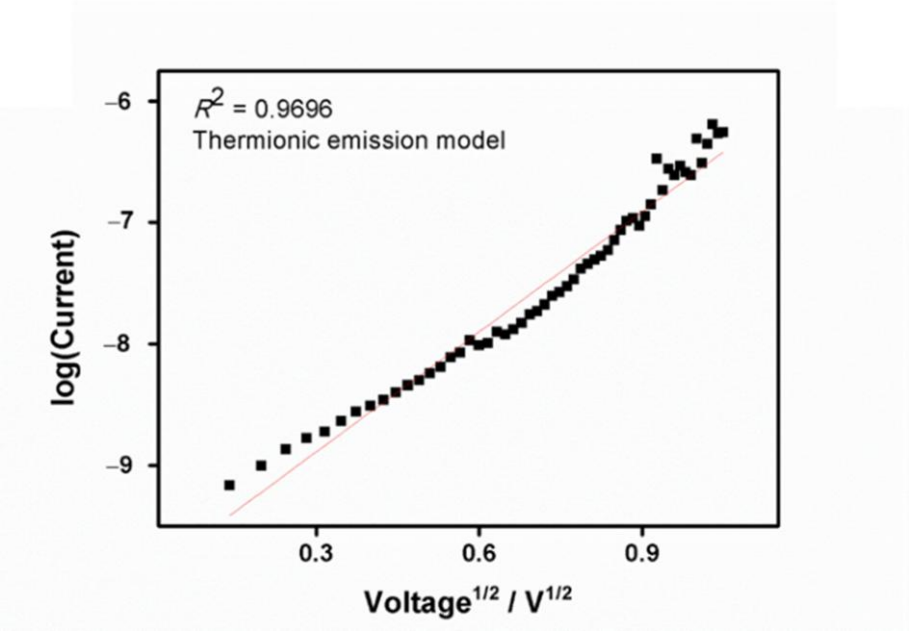

Fig. S43 A plot of ln(*I*) *versus* $V^{1/2}$ using the *I*–*V* characteristics of the OFF state of the device based on **9** (from 0.02 to 1.10 V) and its linear least-squares fit (—).

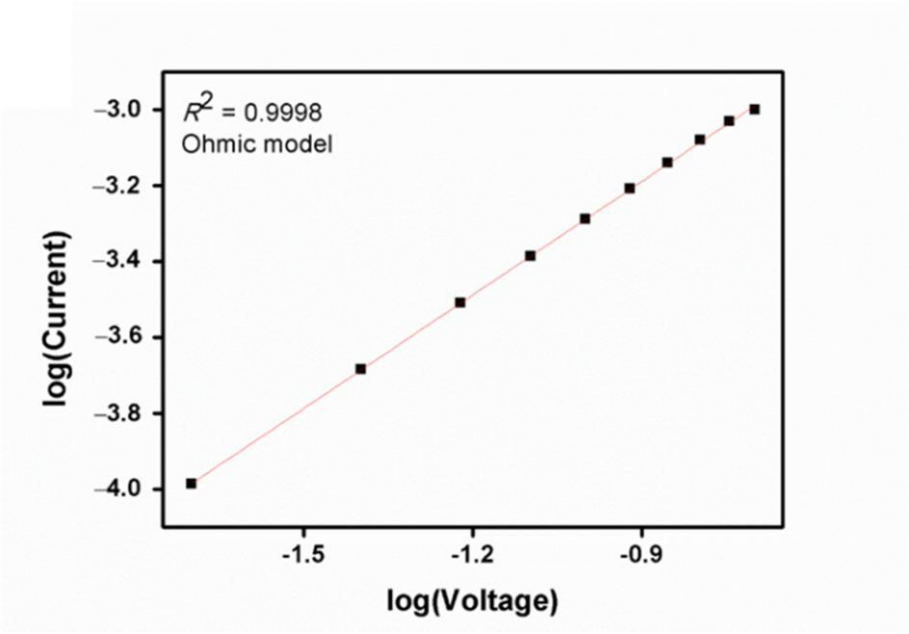

Fig. S44 A plot of ln(*I*) *versus* ln(*V*) using the *I*–*V* characteristics of the ON se of the device based on **9** (from 0.02 to 0.20 V) and its linear least-squares fit (—).

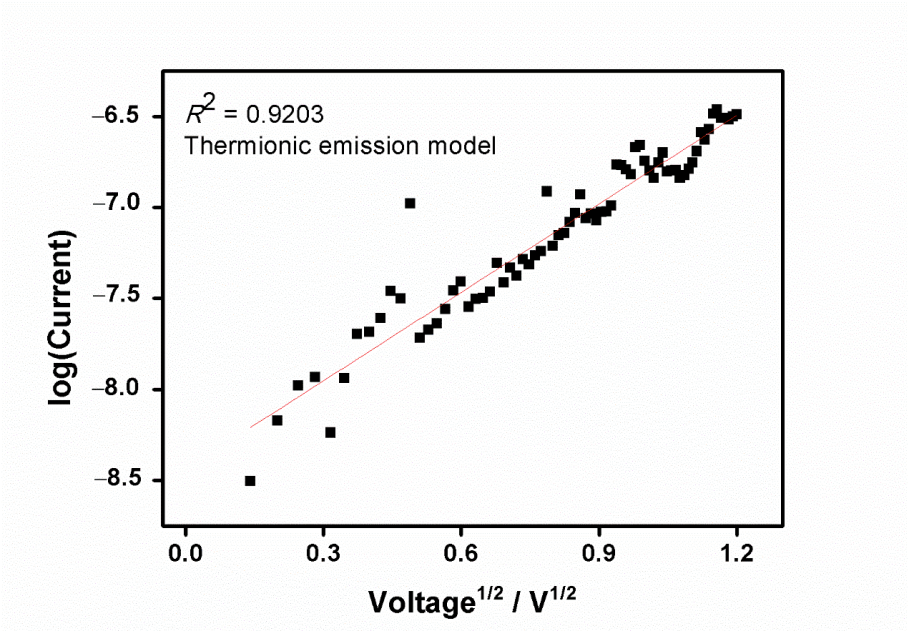

Fig. S45 A plot of ln(*I*) *versus* $V^{1/2}$ using the *I*–*V* characteristics of the OFF state of the device based on **2** (from 0.02 to 1.44 V) and its linear least-squares fit (—).

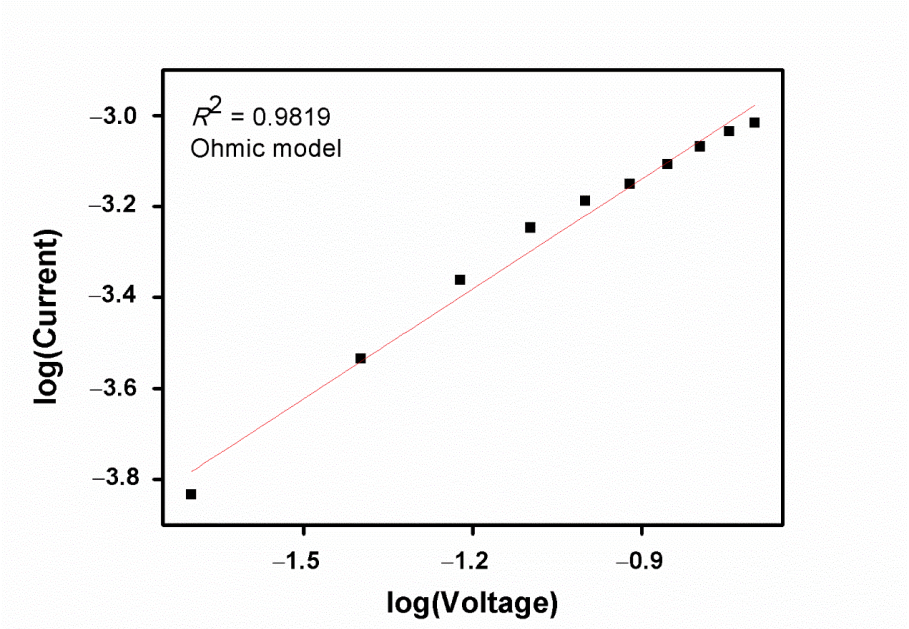

Fig. S46 A plot of ln(*I*) *versus* ln(*V*) using the *I*–*V* characteristics of the ON state of the device based on **2** (from 0.02 to 0.20 V) and its linear least-squares fit (—).

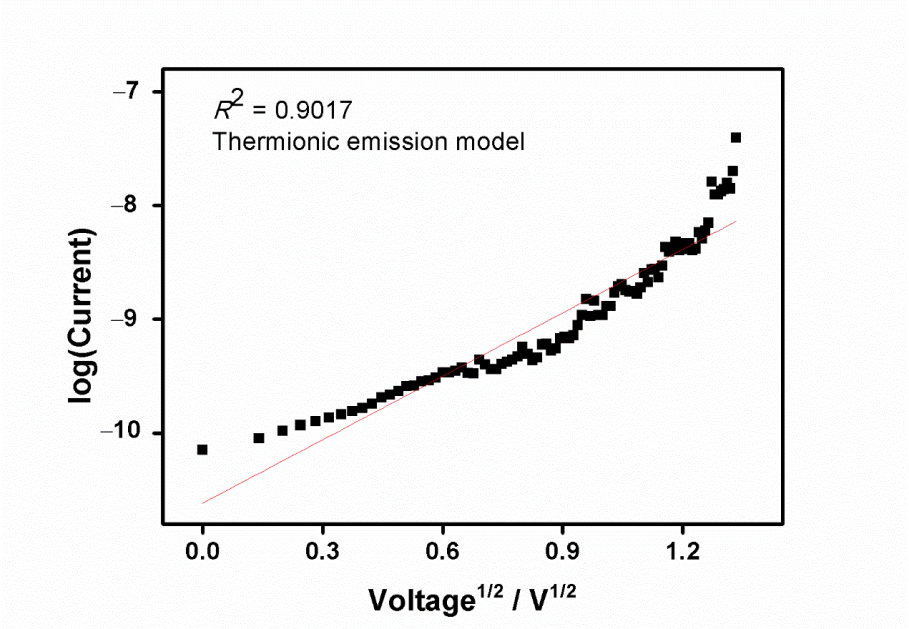

Fig. S47 A plot of ln(*I*) *versus* $V^{1/2}$ using the *I*–*V* characteristics of the OFF state of the device based on **3** (from 0 to 1.78 V) and its linear least-squares fit (—).

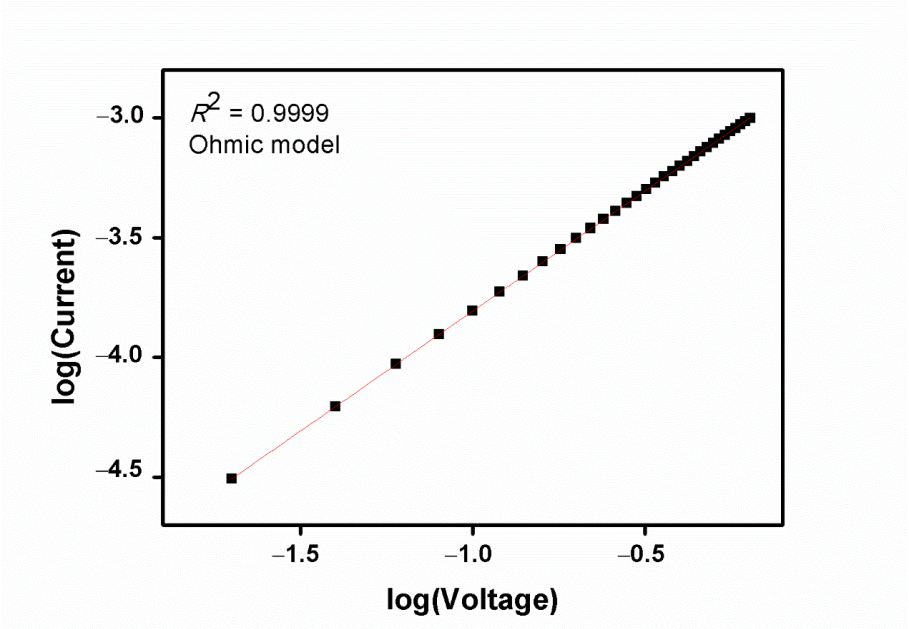

Fig. S48 A plot of ln(*I*) *versus* ln(*V*) using the *I*–*V* characteristics of the ON state of the device based on **3** (from 0.02 to 0.64 V) and its linear least-squares fit (—).

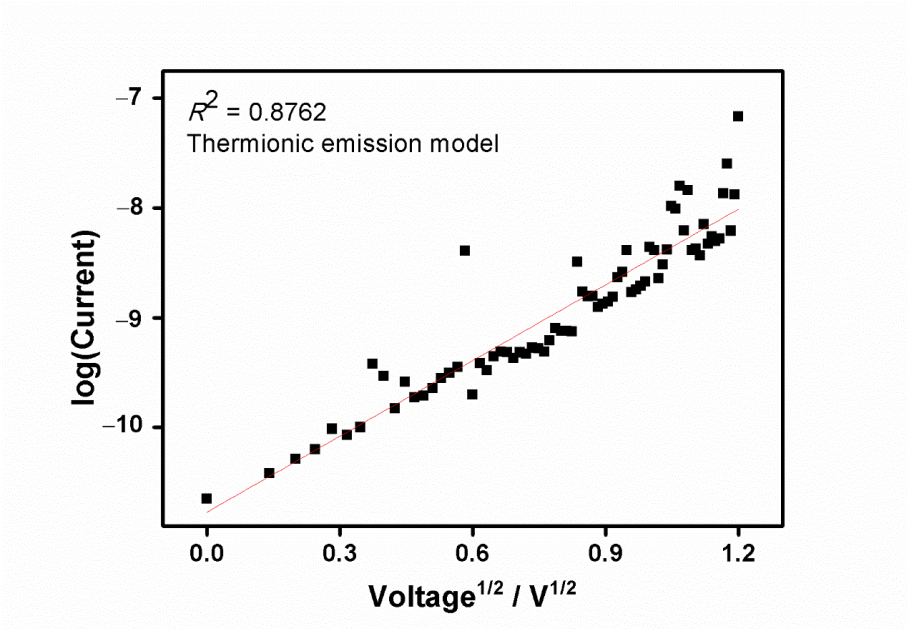

Fig. S49 A plot of ln(*I*) *versus* $V^{1/2}$ using the *I*–*V* characteristics of the OFF state of the device based on **6** (from 0 to 1.44 V) and its linear least-squares fit (—).

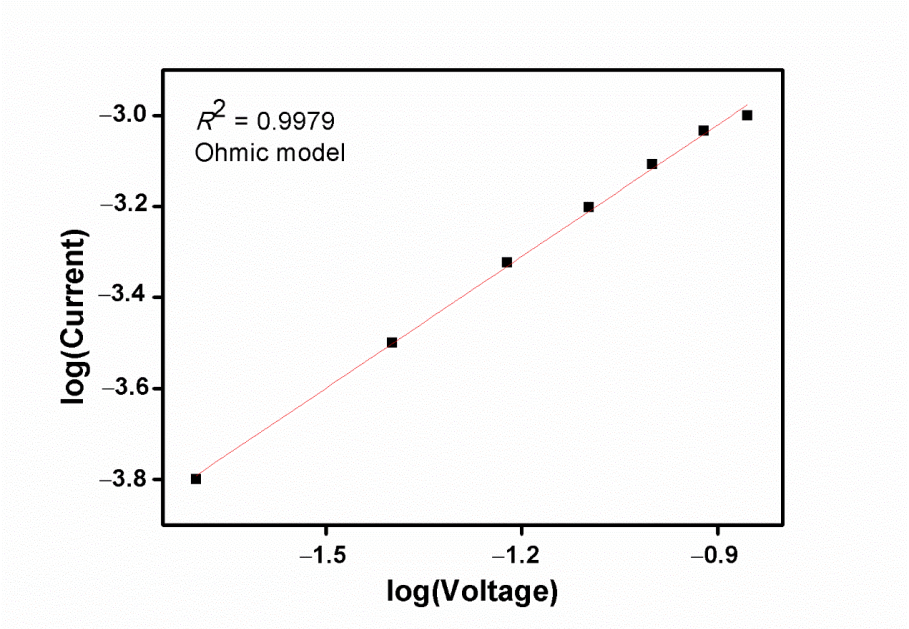

Fig. S50 A plot of ln(*I*) *versus* ln(*V*) using the *I*–*V* characteristics of the ON state of the device based on **6** (from 0.02 to 0.14 V) and its linear least-squares fit (—).

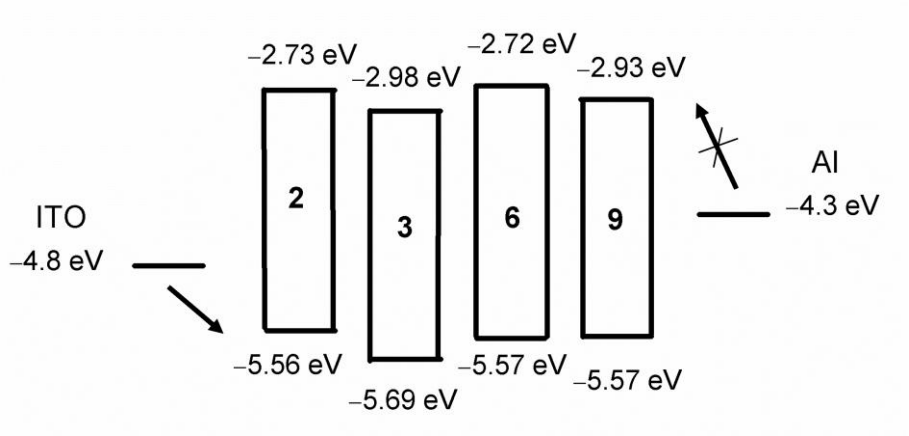

Fig. S51 Schematic diagram of the charge injection process in the memory devices.

Table S1 Crystal and structure determination data of [Pt(**L1**)(DMSO)Cl], **1**, **2** and **6**.

Complex	[Pt(**L1**)(DMSO)Cl]	**1**	**2**·CH_2Cl_2	**6**·$C_5H_{12}O$
chemical formula	$C_{23}H_{19}ClNO_2PPtS_2$	$C_{26}H_{20}NO_3PPtS$	$C_{37}H_{26}Cl_2NO_3PPtS$	$C_{53}H_{60}NO_5PPtS$
M_r	667.02	652.55	861.61	1065.14
T [K]	150	100	102	150
λ [Å]	Mo K_α, 0.71073	Ga K_α, 1.34138	Mo K_α, 0.71073	Mo K_α, 0.71073
crystal system	monoclinic	triclinic	triclinic	triclinic
space group	$P2_1/c$	$P\bar{1}$	$P\bar{1}$	$P\bar{1}$
a [Å]	9.7040(5)	10.2749(6)	11.5125(7)	11.4904(11)
b [Å]	17.0267(8)	10.5551(7)	12.0628(7)	12.2840(11)
c [Å]	13.9056(7)	12.5121(8)	12.9316(8)	18.5318(19)
α [°]	90	68.295(2)	63.928(1)	92.403(3)
β [°]	108.612(2)	74.810(2)	86.338(1)	105.345(3)
γ [°]	90	63.184(2)	78.382(1)	109.248(2)
V [cm^3]	2177.42(19)	1117.74(12)	1579.44(17)	2357.4(4)
Z [$Å^3$]	4	2	2	2
ρ [g cm^{-3}]	2.035	1.939	1.812	1.501
crystal size [mm^3]	0.34 × 0.18 × 0.06	0.31 × 0.21 × 0.20	0.30 × 0.14 × 0.13	0.39 × 0.26 × 0.03
index ranges	$-12 \le h \le 12$, $-22 \le k \le 22$, $-18 \le l \le 18$	$-12 \le h \le 11$, $-12 \le k \le 12$, $-14 \le l \le 14$	$-17 \le h \le 17$, $-18 \le k \le 18$, $-20 \le l \le 20$	$-14 \le h \le 14$, $-15 \le k \le 14$, $-21 \le l \le 22$
reflections collected/unique	42167/5214	11528/3828	43116/12593	54278/9006
GOF on F^2	1.05	1.09	1.14	1.04
final R indices	R_1 = 0.039	R_1 = 0.042	R_1 = 0.042	R_1 = 0.033
[$I > 2\sigma(I)$]	wR_2 = 0.062	wR_2 = 0.120	wR_2 = 0.087	wR_2 = 0.070
largest diff peak and hole [e $Å^{-3}$]	1.33 and –0.84	2.07 and –1.37	1.89 and –1.34	1.45 and –0.80

Table S2 Selected bond distance and angles for [Pt(**L1**)(DMSO)Cl] with estimated standard deviations (e.s.d.s.) given in parentheses

Bond Distances [Å]

Pt(1)–C(7)	2.013(5)	P(1)–C(8)	1.812(5)
Pt(1)–N(1)	2.079(4)	P(1)–C(15)	1.835(5)
Pt(1)–S(2)	2.1961(13)	P(1)–C(16)	1.802(5)
Pt(1)–Cl(1)	2.3676(13)	P(1)–O(1)	1.474(3)

Bond Angles [°]

C(7)–Pt(1)–S(2)	96.60(15)	O(1)–P(1)–C(8)	118.0(2)
C(7)–Pt(1)–Cl(1)	170.71(15)	O(1)–P(1)–C(15)	116.5(2)
C(7)–Pt(1)–N(1)	81.31(18)	O(1)–P(1)–C(16)	116.3(2)
N(1)–Pt(1)–S(2)	171.94(12)	C(8)–P(1)–C(15)	92.7(2)
N(1)–Pt(1)–Cl(1)	92.33(12)	C(8)–P(1)–C(16)	110.3(2)
S(2)–Pt(1)–Cl(1)	90.61(5)	C(15)–P(1)–C(16)	99.2(2)

Table S3 Selected bond distance [Å] and angles [°] for **1** with estimated standard deviations (e.s.d.s.) given in parentheses

Bond Distances [Å]

Pt(1)–C(7)	1.961(8)	P(1)–C(8)	1.806(7)
Pt(1)–N(1)	1.990(6)	P(1)–C(15)	1.820(7)
Pt(1)–O(2)	1.974(5)	P(1)–C(16)	1.807(7)
Pt(1)–O(3)	2.066(5)	P(1)–O(1)	1.486(5)

Bond Angles [°]

C(7)–Pt(1)–O(2)	92.4(3)	O(1)–P(1)–C(8)	120.7(3)
C(7)–Pt(1)–O(3)	173.8(2)	O(1)–P(1)–C(15)	114.7(3)
C(7)–Pt(1)–N(1)	81.5(3)	O(1)–P(1)–C(16)	113.3(3)
N(1)–Pt(1)–O(2)	173.2(2)	C(8)–P(1)–C(15)	92.0(3)
N(1)–Pt(1)–O(3)	93.1(2)	C(8)–P(1)–C(16)	107.8(3)
O(2)–Pt(1)–O(3)	92.8(2)	C(15)–P(1)–C(16)	105.7(3)

Table S4 Selected bond distance [Å] and angles [°] for **2** with estimated standard deviations (e.s.d.s.) given in parentheses

Bond Distances [Å]

Pt(1)–C(7)	1.971(3)	P(1)–C(8)	1.786(3)
Pt(1)–N(1)	2.003(3)	P(1)–C(11)	1.824(3)
Pt(1)–O(2)	2.003(2)	P(1)–C(16)	1.799(4)
Pt(1)–O(3)	2.046(2)	P(1)–O(1)	1.481(3)

Bond Angles [°]

C(7)–Pt(1)–O(2)	95.14(12)	O(1)–P(1)–C(8)	118.47(16)
C(7)–Pt(1)–O(3)	171.05(12)	O(1)–P(1)–C(11)	114.69(16)
C(7)–Pt(1)–N(1)	81.60(13)	O(1)–P(1)–C(16)	114.14(17)
N(1)–Pt(1)–O(2)	175.69(11)	C(8)–P(1)–C(11)	92.39(16)
N(1)–Pt(1)–O(3)	90.27(11)	C(8)–P(1)–C(16)	109.45(16)
O(2)–Pt(1)–O(3)	92.79(10)	C(11)–P(1)–C(16)	105.06(16)

Table S5 Selected bond distance [Å] and angles [°] for **6** with estimated standard deviations (e.s.d.s.) given in parentheses

Bond Distances [Å]

Pt(1)–C(7)	1.979(4)	P(1)–C(8)	1.802(4)
Pt(1)–N(1)	2.004(3)	P(1)–C(11)	1.819(4)
Pt(1)–O(2)	2.051(3)	P(1)–C(16)	1.805(4)
Pt(1)–O(3)	2.013(3)	P(1)–O(1)	1.485(3)

Bond Angles [°]

C(7)–Pt(1)–O(2)	171.01(13)	O(1)–P(1)–C(8)	119.03(17)
C(7)–Pt(1)–O(3)	96.39(14)	O(1)–P(1)–C(11)	115.84(17)
C(7)–Pt(1)–N(1)	81.58(15)	O(1)–P(1)–C(16)	113.50(17)
N(1)–Pt(1)–O(2)	89.97(12)	C(8)–P(1)–C(11)	92.32(18)
N(1)–Pt(1)–O(3)	177.13(12)	C(8)–P(1)–C(16)	109.06(18)
O(2)–Pt(1)–O(3)	91.95(11)	C(11)–P(1)–C(16)	104.47(18)

Table S6 Dynamic light scattering data of **5**–**8** and **10** in 50 % water–THF mixtures at 298 K

Complex	Hydrodynamic diameter / nm
5	234.7 ± 145
6	234.3 ± 130
7	312.9 ± 116
8	228.1 ± 101
10	468.2 ± 161

Table S7 Estimated HOMO and LUMO levels from the electrochemical data of **2**, **3**, **6** and **9**

Complex	HOMO / eV[a]	LUMO / eV[b]	HOMO–LUMO gap / eV
2	–5.56	–2.73	2.83
3	–5.69	–2.98	2.71
6	–5.57	–2.72	2.85
9	–5.57	–2.93	2.64

[a] $E_{HOMO} = -[E_{ox}\,(\text{vs } Fc^{+}/Fc) + 4.80]$ eV.

[b] $E_{LUMO} = -[E_{red}\,(\text{vs } Fc^{+}/Fc) + 4.80]$ eV.

References

1 M. M. J. Smulders, A. P. H. J. Schenning and E. W. Meijer, Insight into the Mechanisms of Cooperative Self-Assembly: The "Sergeants-and-Soldiers" Principle of Chiral and Achiral C_3-Symmetrical Discotic Triamides. *J. Am. Chem. Soc.*, 2008, **130**, 606–611.

2 (a) Written with the cooperation of the program authors Z. Otwinowski, W. Minor: D. Gewirth DENZO: "*The HKL Manuals-A description of programs DENZO, XDISPLAYF, and SCALEPACK*", Yale University, New Haven, 1995. (b) SHELXL97, G. M. Sheldrick, *Programs for Crystal Structure Analysis (release 97–2)*; University of Göttingen, Göttingen, (Germany), 1997.

3 C. Braun, M. Nieger, W. R. Thiel and S. Bräse, [2.2]Paracyclophanes with *N*-Heterocycles as Ligands for Mono- and Dinuclear Ruthenium(II) Complexes. *Chem.–Eur. J.*, 2017, **23**, 15474–15483.

4 Q. Chu, M. Makhlouf Brahmi, A. Solovyev, S.-H. Ueng, D. P. Curran, M. Malacria, L. Fensterbank and E. Lacôte, Ionic and Organometallic Reductions with *N*-Heterocyclic Carbene Boranes. *Chem.–Eur. J.*, 2009, **15**, 12937–12940.

5 S. Debnath, R. R. Ujjwal and U. Ojha, Self-Healable and Recyclable Dynamic Covalent Networks Based on Room Temperature Exchangeable Hydrazide Michael Adduct Linkages. *Macromolecules*, 2018, **51**, 9961–9973.

6 V. N. Kozhevnikov, M. M. Ustinova, P. A. Slepukhin, A. Santoro, D. W. Bruce and D. N. Kozhevnikov, From 1,2,4-Triazines towards Substituted Pyridines and their Cyclometallated Pt complexes. *Tetrahedron Lett.*, 2008, **49**, 4096–4098.

7 Y. Dienes, S. Durben, T. Kárpáti, T. Neumann, U. Englert, L. Nyulászi and T. Baumgartner, Selective Tuning of the Band Gap of π-Conjugated Dithieno[3,2-b:2′,3′-d]phospholes toward Different Emission Colors. *Chem.–Eur. J.*, 2007, **13**, 7487–7500.